POLITECNICO DI MILANO

MASTER THESIS

A Radiation Model for Power Degradation Estimation in Earth Centered Satellites

Author:
Alberto MAÑERO CONTRERAS

Supervisor:
Dr. Francesco TOPPUTO
Co-Supervisor
Simone CECCHERINI

SCHOOL OF INDUSTRIAL AND INFORMATION ENGINEERING

DEPARTMENT OF SCIENCES AND AEROSPACE TECHNOLOGIES

July 13, 2018

POLITECNICO DI MILANO

Abstract

Department of Sciences and Aerospace Technologies
School of Industrial and Information Engineering

A Radiation Model for Power Degradation Estimation in Earth Centered Satellites

by Alberto MAÑERO CONTRERAS

ELECTRIC propulsion systems meant an important improvement in the space sector ever since it was invented. Lately, it has been tested in different applications and it holds capital advantages over the conventional propulsion systems. On the other hand, low-thrust transfers performed with electric propulsion require large times of flight. A major drawback comes along with this fact: high exposure to trapped energized particles in Van Allen Belts. This radiation environment becomes a considerable issue for electronic systems and satellite onboard equipment, as well as a relevant solar array degradation, which implies a significant loss of power capability during the mission. The current thesis focuses on the implementation of a fast and reliable radiation model that is meant to be incorporated into an optimization framework in order to minimize the above-mentioned deterioration of the photovoltaic cells along an Earth-centered trajectory. The developed model has been validated with the AE9/AP9/SPM tool and SPENVIS, and the basis for the aforementioned optimal control has been stated.

POLITECNICO DI MILANO

Sommario

Department of Sciences and Aerospace Technologies
School of Industrial and Information Engineering

A Radiation Model for Power Degradation Estimation in Earth Centered Satellites

by Alberto MAÑERO CONTRERAS

I sistemi di propulsione elettrica hanno significato un importante miglioramento nel settore spaziale. Recentemente, la propulsione elettrica è stata utilizzata per diverse applicazioni ed offre sostanziali vantaggi rispetto ai convenzionali sistemi di propulsione. D'altra parte, i trasferimenti a bassa spinta, tipici degli attuali sistemi propulsivi elettrici, richiedono alti tempi di volo. Di conseguenza, un inconveniente rilevante è dovuto all'esposizione del satellite alle particelle ad alta energia all'interno delle fasce di Van Allen. Il passaggio all'interno di questo ambiente diventa un considerevole problema per quanto riguarda i sistemi e le apparecchiature all'interno del satellite; inoltre, può portare ad una rilevante degradazione dei pannelli solari che a sua volta implica una significativa perdita di generazione di potenza durante la missione. La presente tesi si concentra sullo sviluppo di un modello veloce e rappresentativo per quantificare l'esposizione alle suddette radiazioni, in modo tale da poter essere utilizzato in un processo di minimizzazione del deterioramento delle celle solari lungo una traiettoria in un sistema centrato nella Terra. Il modello prodotto è stato validato attraverso il software AE9/AP9/SPM e con SPENVIS; al contempo, le basi per sviluppare il suddetto controllo ottimo sono state derivate.

Acknowledgements

First of all, I would like to express deepest gratitude to my advisor Prof. Dr. Francesco Topputo for his support, guidance, understanding and encouragement throughout my study and research. Secondly, I owe special recognition to Simone Ceccherini. Without his incredible patience and timely wisdom and counsel, my thesis work would have been a frustrating and overwhelming pursuit.

Now that my student episode approaches to its end, I would like to dedicate some lines to the core of my success: my family. Papá, mamá y hermanita. Ya sabéis que no hay palabras de agradecimiento que describan la gratitud que siento por vuestro apoyo incondicional durante estos ocho largos años. Porque gracias a vosotros, entendí que no importa el número de veces que caigas, mientras siempre te levantes una más. Porque cuando no creí en mi mismo, vosotros fuisteis los que me disteis una inyección de fe. Estoy tremendamente orgulloso de la educación que me habéis proporcionado y de las oportunidades de las que he podido disfrutar gracias a ello. Gracias de corazón.

Furthermore, I would like to acknowledge many people from Milan, but especially, those ones closest to me during these two years. Mohit, Aroon, and Semih. Thank you guys for being a constant in the happiest moments, but most importantly, the saddest ones. It would have been very tough without you all.

I owe special gratitude to my flatmates. They have made me feel comfortable at home and they are the ones who heard my screams and the manic laughters while working on this thesis. Andrés, Yasmina, and especially María, whom I have shared with these two years. Thank you all for your support.

En un párrafo aparte, hago mención a los *bicchieri*. Habéis aparecido tarde, pero habéis sido una bendición. Os podría agradecer muchas cosas, pero en especial, gracias por aguantar mis turras sempiternas sobre la tesis. Habéis sido un pilar fundamental estos meses y espero que esta amistad se prolongue en el tiempo con más planes en la Península Ibérica.

Para acabar, como no podía ser de otra manera, me acuerdo de vosotros: *los buhítos*. Porque aunque estemos lejos, crezcamos y cada uno de nosotros tomemos caminos diferentes, nunca dejaréis de ser el motor de mi vida. Gracias a todos y cada uno de vosotros, de corazón, por haberme enseñado lo que significa la amistad.

Contents

List of Figures

List of Tables

Notation

$\mathbb{R}^n$	n-dimensional Euclidean space
$\mathbb{R}^{n\times m}$	Matrices of dimension $n \times m$
$\lvert\cdot\rvert$	Magnitude of a vector
$\lvert\mathbf{A}\rvert$	Determinant of the square matrix $\mathbf{A}$
∇	Gradient of a vector
log	Natural logarithm of a vector/matrix
$*$	Optimal variable
c	Exhaust velocity
$D_{e,p}$	Relative Damage Coefficient
E	Energy level
g_0	Gravitational acceleration at sea level
G	Universal gravitational constant
G_r	Total equivalent flux at 1 MeV
h_k	Altitude value at iteration k
H	Hamiltonian
I_{sc}	Cell short circuit intensity
I_{sp}	Thruster specific impulse
J	Performance index of the optimal problem
J_d	Julian days
J_r	Total equivalent fluence at 1 MeV
L	Lagrangian
m	Mass of the spacecraft
M_E	Mass of the Earth
P_{max}	Cell maximum power
R_E	Radius of the Earth
S_r	Switching function for radiation optimal problem
u	Control variable
V_{oc}	Cell open circuit voltage
$\mathbf{F_e}$	Matrix of electrons differential flux
$\mathbf{F_p}$	Matrix of protons differential flux

$\mathbf{g}$	Gravitational acceleration for the restricted two-body problem
$\mathbf{I_{n\times m}}$	Identity matrix $n \times m$
$\mathbf{J_\Gamma}$	Jacobian of the shooting function
$\mathbf{r}$	Position vector
$\mathbf{T}$	Thrust vector
$\mathbf{v}$	Velocity vector
$\mathbf{x}$	State vector
$\mathbf{y}$	Augmented state-costate vector
$\mathbf{z}$	Augmented state-costate-STM vector
α_{p-e}	Proton-electron conversion parameter
$\boldsymbol{\alpha}$	Thrust direction unit vector
$\boldsymbol{\Gamma}$	Shooting function
δ	Altitude step size
Θ	Term related with the BC on the states and the terminal cos function
κ	Cell coverglass thickness
$\boldsymbol{\lambda}$	Costates vector
μ	Earth gravitational constant
$\boldsymbol{\nu}$	Lagrange multipliers for the terminal BC
$\boldsymbol{\Xi}$	State Transition Matrix
ϕ	Omnidirectional integral flux
$\boldsymbol{\Phi}$	Omnidirectional integral fluence
$\boldsymbol{\Psi}$	Terminal function of the states

Acronyms

COV	**C**alculus **O**f **V**ariations
EFT	**E**quivalent **F**luence **T**heory
EP	**E**lectric **P**ropulsion
GEI	**G**eocentric **E**quatorial **I**nertial
GEO	**G**eostationary **E**arth **O**rbit
GRS	**G**eographic **R**eference **S**ystem
GTO	**G**eostationary **T**ransfer **O**rbit
IGRF	**I**nertial **G**eomagnetic **R**eference **F**ield
IRENE	**I**nternational **R**adiation **E**nvironment **N**ear **E**arth
IVP	**I**nitial **V**alue **P**roblem
LEO	**L**ow **E**arth **O**rbit
LT2O	**L**ow **T**hrust **T**rajectory **O**ptimization
MAG	Geo**mag**netic
NEO	**N**ear **E**arth **O**bjects
PMP	**P**ontryagin **M**inimum **P**rinciple
RAAN	**R**ight **A**scending of **A**scendent **N**ode
RDC	**R**elative **D**amage **C**oefficient
RK	**R**unge **K**utta
SAA	**S**outh **A**tlantic **A**nomaly
SEP	**S**olar **E**lectric **P**ropulsion
SPENVIS	**SP**ace **ENV**ironment **I**nformation **S**ystem
STM	**S**tate**T**ransition **M**atrix
TOF	**T**ime **O**f **F**light
TPBVP	**T**wo-**P**oint **B**oundary-**V**alue **P**roblem

Dedicated to my parents and sister, Alberto, Lola and Julia, whom I love tenderly.

Chapter 1

Introduction

"One small step for man, one giant leap for mankind."

- Neil Armstrong, *Apollo 11*

OCTOBER the 4th, 1957. History changed from this day forward when the Soviet Union successfully launched the worldwide known Sputnik I. Some decades after, it is simple to figure how this historical fact impacted a wide range of fields that ushered in new political, military, technological and scientific developments. Most of them were framed during the few following years from Sputnik's launch, the Cold War, while space would become another tense arena for this peculiar race, as each side sought to show its great potential and superiority at all possible levels. Barely four months later, the U.S. launched its own artificial satellite, the Explorer I, as a clear opposing argument from the Soviet Union's aspirations to conquer the space. This satellite is of particular interest for this thesis because it was the first spacecraft to detect the Van Allen Radiation Belt, named after its discoverer James Van Allen, returning data until its batteries were exhausted after nearly four months[1]. In the same year, the President of the United States of America Dwight Eisenhower signed a public order prior to creating the National Aeronautics and Space Administration (NASA), the well known federal agency dedicated to space exploration. Even though the Soviet Union took another step forward sending Yuri Gagarin as the first man to orbit the Earth in April 1961, the United States effectively 'won'the space race by landing successfully on the moon the 20th of July 1969 aboard the Apollo 11, setting the end of a period that left a trace in history.

Almost five decades later, the space sector has experienced an enormous growth. Many other countries have carved their own spot in space as a

[1] https://www.nasa.gov/mission_pages/explorer/explorer-overview.html last visited on 15th of May, 2018.

way to demonstrate their capabilities of increasing their space activity. Currently, there are thousands of satellites orbiting the Earth while the launch rate is growing. There is a great selection of space applications, ranging from telecommunications to Earth observations. Even though their goals could be diverse, the trajectory analysis and optimization techniques play always a major role.

A trajectory is defined as the path that a moving object follows through space as a function of time. Their applications are mainly placing a satellite into a predefined orbit or either make an orbital transfer from two different orbits. Historically, the study of trajectories has caught the eye of many engineers, especially the study of those that optimize a quantity that normally has a large impact on the overall mission, economically or another kind, such as *time, fuel* or, as this thesis reports, *radiation*. Those trajectories are called optimal ones.

Another way to distinguish two trajectories resides on the kind of primary propulsion used by the spacecraft. They are broadly divided into two main branches: high-thrust and low-thrust transfers. For the first group, the main propulsive capability of the spacecraft comes from chemical rockets that are modelled as producing instantaneous (ideal) changes of velocity. On the other hand, low-thrust transfers are accomplished through engines that use electrical power to accelerate a propellant and, consequently, to apply a change of velocity to the spacecraft in a very efficient manner; the Electric Propulsion (EP) systems. Even though the idea of electrical propulsion dates back to 1911, it was not developed until 1964 when the experimental satellite SERT-1[2] was launched with an ion engine aboard, operating for 31 minutes. Its follow-up mission was launched six years later under the name of SERT-2[3]. Nonetheless, high-thrust solutions were more frequently implemented in practical missions at this time due to the not sufficient development of the low-thrust technology. Gradually, EP technology has been improved and refined. As a result, its applications have been shifted from station keeping (the first application it had) to primary propulsion solutions. Moreover, it provides many advantages over the conventional propulsion systems. For example, due to the low propellant consumption, electrical propulsion systems aim at a greater payload fraction, cheaper launchers and longer missions. Furthermore, they provide a precise pointing because of their low highly controllable thrust [1]. Unfortunately, the transfers made with this type of propulsion takes very high Times of Flight (TOF), in the order of

[2] https://www.grc.nasa.gov/WWW/ion/past/60s/sert1.htm last visited on 20th of May, 2018.

[3] https://www.grc.nasa.gov/WWW/ion/past/60s/sert2.htm last visited on 20th of May, 2018.

months depending on the initial and final orbits, and the control authority. Great examples of this technology are the ESA's SMART-1[4] which was used to test solar electric propulsion and other deep-space technologies, while performing scientific observations of the Moon, and the ESA's Lisa Pathfinder[5] (also called SMART-2), which paved the way of future missions by testing in flight the very concept of gravitational wave detection.

Keeping the idea of gathering energy from the Sun as a method to feed the propulsion system, the full development of the Solar Electric Propulsion (SEP) systems becomes particularly important for future space missions, such as NASA Asteroid Robotic Redirect Mission, which will be designed to capture a large (up to 1000 metric ton) boulder from the surface of a Near Earth Asteroid, and bring it into high lunar orbit [2].

1.1 Low-Thrust Optimal Trajectories

During the analysis and design of space missions, some of the most important tasks are the design and optimization of the transfer path. As stated in [3], trajectory optimization problems that involve high-thrust propulsive systems are typically formulated as discrete optimization problems and generally are well-conditioned from the numerical point of view, however, low-thrust systems operate for large periods of the mission continuously and its associated optimal control problems are numerically ill-conditioned in most of the cases. This thesis mainly focuses on the development of a model of the radiation environment for Earth centered satellites as well as the formulation of the radiation optimal trajectories for low-thrust transfers. Generally, the computation of a spacecraft's trajectory, particularly the optimal one, is made through the integration of a set of differential equations which represents its dynamics. The terms included in this set of equations normally account for the inertial forces acting on the system as well as other terms linked to control variables such as the thrust, along with its direction, for instance. Hence, the optimal trajectory is the output of an optimization of those control variables.

As mentioned before, problems regarding high-thrust propulsion systems can be modeled as discrete ones due to the fact that their propulsive performances are bounded in short periods of time, justifying accordingly the fact of the discretization done. Generally, they are straightforward to solve if compared with the low-thrust problems. These latter ones, contrarily, bring complications when it comes to find an optimal solution due to the fact that they do not perform instantaneously. Thus, the optimal solutions of this

[4] http://sci.esa.int/smart-1/ last visited on 9th of July, 2018
[5] http://sci.esa.int/lisa-pathfinder/ last visited on 20th of May, 2018

type of problems require tools based on continuous optimization techniques that model the control variables as continuous functions in order to solve the problem appropriately.

Low-thrust optimized trajectories are typically obtained through either indirect or direct methods [42]. Direct methods entail the parametrization of the problemand the use of nonlinear programming techniques to optimize an objective function by adjusting a set of variables. They offer a wide range of advantages because of their robustness and simplicity. Nonetheless, their weak points are both the great amount of time needed to achieve a solution and their poor accuracy which comes along with them. For more information about direct methods, the reader is referred to [4].

Alternatively, indirect methods are based on Calculus of Variations (COV). Classical solutions to minimization problems in the calculus of variations are prescribed by boundary value problems involving certain types of differential equations, known as the associated Euler–Lagrange equations. The mathematical techniques that have been developed to handle such optimization problems are fundamental in many areas of mathematics, physics, engineering, and other applications. In addition, another principle used to handle an optimization problem via indirect methods is the Pontryagin Minimum Principle (PMP), which exploits the Euler-Lagrange equations. These two tools are used to transform the original problem to a reduced one, depending only on few parameters. This is done by adding constraints represented by Lagrange multipliers $\boldsymbol{\lambda}(t)$ which are utilized to derive the necessary conditions for an extremum considering the variation of the performance index J. Given that the low-thrust optimal trajectory problems are optimized over time continuously, it is straightforward to understand that the Lagrange multipliers, or costates, are going to be governed by a set of differential equations which will have to be integrated over time. Hence, the conditions for a continuous optimal problem are composed by the ones subjected to the costates $\boldsymbol{\lambda}(t)$ as well as the ones linked with the state of the system, $\boldsymbol{x}(t)$. Once these conditions are derived, the original problem results in a Two-Point Boundary-Value Problem (TPBVP) that is solved by satisfying the conditions commented above. Indirect methods were named after this fact - solving the canonical problem by transforming it into a TPBVP. Nevertheless, these indirect methods are subject to extreme sensitivity to the initial guess of the variables - some of which are not physically intuitive, a fact that comprehends its main disadvantage.

A proper mathematical definition gathering the concept is required once a brief introduction about the low-thrust optimal problem has been given. As stated in [5], this definition reads

Definition 1. An optimal control problem consist on the computation of the state vector $\boldsymbol{x}(t) \in \mathbb{R}^n$, the costates vector $\boldsymbol{\lambda}(t) \in \mathbb{R}^n$ and the control $\boldsymbol{u}(t) \in \mathbb{R}^m$ based on boundary conditions that optimize some cost function J.

It is of capital importance to dedicate some introduction lines to the cost function J. As explained in [6], when determining the optimal trajectory, this performance index J is not always the same. Sometimes, one requirement sets the minimization of the required propellant, giving rise to the *minimum fuel problem*. In order to solve that problem, it is needed an estimation of the upper bound of the total transfer time. For that reason, one must solve first the *minimum time problem*. When one addresses the *minimum radiation problem*, the same estimation of the final time is a requisite as well. This topic will be covered extensively in Chapter 4.

1.2 Motivation of the Thesis

In Section 1.1 the complexity of solving the optimal low-thrust transfer has been introducted. It does not just comprehend to solve the problem under study subjected to some constraints, but doing it while minimizing a certain cost function to reach the optimal solution. This thesis consists in a follow-up study about these family of optimal trajectories done already for a minimum TOF [6, 9], and minimum fuel consumption [7]. As commented previously, the main motivation of this thesis is to compute the trajectory profile that optimizes the radiation absorption, taking into account a model developed with the Space Environment Information System (SPENVIS[6]) and AE9/AP9/SPM[7] tool, which will be entirely explained in Chapter 3.

Therefore, this thesis was conceived to propose a family of solutions for orbital transfers from diverse LEOs to GEO. It is important to remark that, in opposition to other studies [23], in this thesis, there is going to be only one single transfer orbit which will connect a certain LEO with the GEO. There will not be any hybrid transfer or switching orbit in which both high and low-thrust phases are present, but only the latter one. To clarify this explanation, a scheme of the transfer is depicted in the Figure 1.1. Of course, the transfer represented by the dashed line is going to be one of the goals of this thesis, so it is not representative neither realistic the way it is depicted in the picture.

This minimum radiation maneuver turns out to be very interesting because under the light of the facts previously explained one would think that minimum time and minimum radiation problems are inevitably related. As a

[6]The Space Environment Information System. Website: https://www.spenvis.oma.be/ last visited on 10th of July, 2018.

[7]Radiation Belt and Space Plasma Specification Models. Website: https://www.vdl.afrl.af.mil/programs/ae9ap9/ last visited on 10th of July, 2018.

matter of fact, it is very straightforward to think that the more the spacecraft holds into the Van Allen Belts, the more radiation it receives. Hence, in a preliminary study, both problems must be linked somehow. This topic will be cover in Chapter 4 while analyzing the statement of the problem.

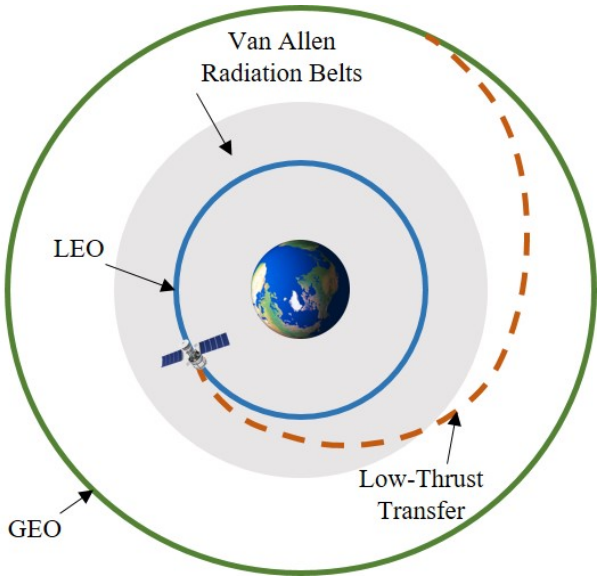

FIGURE 1.1: Typical orbital transfer from LEO to GEO.

Once again, the final aim of this thesis is to compute the optimal trajectory which minimizes the radiation received by the spacecraft. In the next Chapter, the radiation environment is deeply investigated, but it is important to comment beforehand in a briefly manner the harsh effects of the radiation on the spacecraft. One variable of capital importance is the Total Ionizing Dose. The term, total ionizing dose, implies the dose is deposited to the electronics through ionization effects only. As stated in [8], the energy deposited by radiation moves the electrons to a higher energy state, thus making them available for conduction and mobile inside a nonconductive material. These electrons, or more correctly the positive charge created by ionization, are the prime cause of the total ionizing dose effects. This ionizing dose not only affect to the electronics of the spacecraft, it also can affect a great variety of equipment types and devices such as optics, electro-optics, photovoltaics, thermal and optical coatings, for instance. It can also damage biological systems, especially astronauts, but that consideration does not play any role in this study because the system is unmanned; a satellite.

In order to solve the problem, a robust solver is needed. The one which has been used during this research consists on an updated version of the Low-Thrust Trajectory Optimization (LT2O) solver developed by Politecnico di Milano [7, 9, 10]. The modifications included in this solver have been the

addition of a radiation module for taking into account the fluence of particles along the trajectory of the satellite.

1.3 Goals of the Thesis

The main targets of this thesis are mostly two. In the first place, to develop an accurate and fast radiation model that represents and accounts faithfully for the protons/electrons of a certain energy range present at the Van Allen Belts which the spacecraft would encounter during the transfers under study through variables such as the fluence or the flux. Some verifications must be done in order to double check the model and its efficiency should be questioned as well. Along with that, its simplifications and assumptions must be properly justified, as well as the shortages adjoined to them.

Secondly, once the model has been properly verified and checked, the next potential step is to analyze how the low-thrust optimal control problem can be solved, so implementing a new module into the existent solver of minimum time and minimum fuel problems. The solution for different transfer orbits must be studied, typically from several Low Earth Orbits (LEO) to the Geostationary Earth Orbit (GEO). Finally, a trade-off comparing minimum time, minimum fuel and minimum radiation transfer orbits must be done and their differences pointed out.

1.4 State of the Art

Once the main topics of this thesis have been concisely explained, the state of the art of such technology is analyzed in this Section. For example, recent studies indicate new solutions for optimal low-thrust trajectories for SEP [11]. There are mainly three topics which this thesis focuses on, namely radiation environment; how it affects the satellite systems through the model that has been developed, orbital transfers, in particular from LEO to GEO, and the different types of solvers used currently to deal with these kinds of problems.

It is well known the huge impact that a harsh environment like the one present in the outer space could have on the most sensitive devices of the spacecraft if they are not well isolated against radiation. From an engineering perspective, these effects are important in determining the reliability of electronics to the ionizing dose environment, for example. Estimations on these effects have been studied for many years in order to be able to preserve their functionality in the radiation environment found in space [8, 12, 13]. A lot of effort has been invested as well in the matter of modeling this environment from the numerical point of view, giving rise to several models which have been

applied to studies to achieve diverse goals. For example, the research in [14] accounts for a minimization of the proton displacement damage dose during electric orbit raising of satellites. A study about radiation optimal transfer from GTO to GEO with EP is presented in [15]. Contrarily, in the work referenced in [16], some radiation damage constraints are imposed to perform a minimum fuel electric orbit raising. Nevertheless, due to the fact that this thesis is mainly inspired on the effects which have the Van Allen Belts on the trajectory of the spacecraft, it is mandatory to mention a thorough guide [17] from which the thesis has been inspired.

Nowadays, launcher vehicles do not place electric satellites in GEO straightaway. Normally, they are located in orbits closer to the Earth from which they are able to do the transfer. Generally, these intermediate orbits are either LEO or Geostationary Transfer Orbits (GTO). Therefore, these orbits are the initial point from which the low-thrust maneuver takes place. Focusing on the LEO to GEO transfers [18], even though their transfer times are very high, they are attainable according to [19] by following spiral strategies which allow performing the transfer without the need of any optimization tool. In [20], the matter of low-thrust spiral trajectories is studied into detail. Instead, if one looks at transfers done from GTO to GEO, the field of study is much wider, justifying the fact that these kinds of transfers are more practical from the operational point of view [21, 22, 23]. Low-thrust maneuvers are not just utilized for transfers from LEO or GTO to GEO. The research on this topic evolves further over time and there are already some studies in which low-thrust propulsion systems are used for reaching orbits around the moon [24, 25, 26, 27, 28]. Homologue studies exist for interplanetary orbits using low-thrust performance as well [29, 30].

The existing methods to solve the wide variety of problems described above are almost endless. As explained in [6], most of them have limitations in terms of accuracy or generalization, as they do not offer a wide range of possible applications. Even though covering them all is a task nearly impossible to achieve, it deserves special mention the standard numerical one developed in the 70s by Lester L. Sackett (and his associates) while he was at MIT Lincoln Labs: SEPSPOT. The program computes optimal planetocentric trajectories using the techniques of optimal control and orbital averaging [31].

1.5 Structure of the Thesis

This document is organized and structured as follows:

- **CHAPTER 2** gives an overview of the radiation environment in which lays the groundwork of the following Chapters. In the beginning, some

transversal general concepts are presented as well as the reference frames which are used to develop the radiation model explained in the next Chapter. Before explaining the Van Allen Radiation Belts, which is one of the main notions of this thesis, a wide detailed outline of the diverse types of radiation is described. Finally, a degradation model of the solar cells is given in order to measure and estimate the total equivalent fluence, which is going to be the variable to minimize under this study, in other words, the shooting function.

- **CHAPTER 3** introduces the radiation model used throughout this thesis in order to build the aforementioned shooting function to minimize the total equivalent fluence during its optimal trajectory. Goals of the model are presented along with the assumptions and simplifications which have been done. Listed afterward are the known issues and limitations of this model.

- **CHAPTER 4** provides the mathematical basis of the thesis. It describes the dynamic model of the system and the statement of the problem, deriving the constraints needed to solve it. In addition, a full review of optimal control theory has been included. The structure of the solver which has been used for the analysis is briefly outlined and the radiation optimal problem has been stated. Some validations of the model used confronting with SPENVIS and AE9/AP9/SPM tool have been reported. Lastly, some preliminary results of the thesis are stated to finalize the Chapter.

- **CHAPTER 5** summarizes the main findings of this research and it includes a set of recommendations for future work.

Chapter 2

The Radiation Environment

"This is Major Tom to Ground Control..."

- David Bowie, *Space Oddity*

THE concept of radiation in space was born less than seventy years ago once the Van Allen Belts were detected for the first time in history. Before that time, the only manifestations of the presence of radiation in space were unexplained phenomena such as the aurora borealis or the deformation of the ionized tail of comets caused by the solar wind [32]. Nowadays, the field of space radiation has been extensively studied and its sources completely understood, even though there are still some questions that Science must find the answers to, for instance the high-energy cosmic rays[1].

Life on Earth is well protected from deep space's environmental threats by mainly three different mechanisms: the Earth's atmosphere, the Earth's magnetic field and the solar winds. They will be explained in Section 2.1 along with the different types of radiation encountered in deep space. This environment degrades electronic systems and onboard equipment, in particular, and creates radiobiological hazards during manned space flights [32, 33]. Therefore, as new missions arise with the aim of exploring barely known deep space's locations, such as Mars, other exoplanets (like Kepler[2], which is a space observatory launched by NASA in 2009 to discover Earth-size planets orbiting other stars), or Near Earth Objects[3] (NEO), the satellites will face lengthened radiation exposure once they abandon the atmosphere.

This Chapter provides a brief introduction of the concepts brought in above and its main goal is to make the reader familiar with some theory of capital

[1] https://goo.gl/LxgcgU last visited on 27th of May, 2018

[2] https://www.nasa.gov/mission_pages/kepler/overview/index.html last visited on 27th of May, 2018

[3] Near-Earth Objects are comets and asteroids that have been nudged by the gravitational attraction of nearby planets into orbits that allow them to enter the Earth's neighborhood.

importance regarding the radiation environment that will serve as the base for the following Chapters.

2.1 Types of Radiation

In the last paragraphs, the concept of radiation has been introduced and its main effects shortly explained. Thus, the next logical step is to describe the different sources of radiation that a spaceship would encounter once it travels to the outer space, far away from the natural protection of the Earth's atmosphere. At this point, it is crucial to remark the two principal groups in which radiation is divided. The *non-ionizing radiation* is the one in which particles impart energy on to the atoms and molecules with which it interacts but does not strip off electrons, so it does not harm radiosensitive devices by itself. Hence, it has not been taken into account for the sources listed below. Furthermore, it is cataloged into a low energy radiation category and it is the easiest to protect aganist[4] (UV radiation, for instance). On the contrary, *ionizing radiation* deposits energy onto the atoms and molecules with which it interacts, causing electrons to be lost. The resulting ions, or charged particles, give this form of radiation its name. They can be identified mainly as three:

- **Galactic Cosmic Rays:** they are created outside the solar system. They are composed of ionized atoms, independently of their number of protons. Despite their associated very low flux levels, they contribute to severe ionization once passed through matter due to their fast velocity (close to the speed of light) and their heavy element composition. For the most part, the Earth's magnetic field provides shielding for spacecraft from galactic cosmic radiation. However, cosmic rays have free access over the polar regions where the magnetic field lines are open to interplanetary space[5].

- **Solar Cosmic Radiations:** consist of two components, the low energy solar wind particles that flow constantly from the sun, and the highly energetic *Solar Particle Events* which are mainly high energy electrons, protons and alpha particles ejected into space. Prior to the coronal mass ejections present at the neighborhood of solar flares (Figure 2.1), the interplanetary shock waves boost these particles up almost to the speed of light.

[4] https://goo.gl/7jbXbP last visited on 27th of May, 2018

[5] https://srag.jsc.nasa.gov/spaceradiation/What/What.cfm last visited on 27th of May, 2018

- **Trapped Radiation:** referred normally as Van Allen Belts, it consists of energetic electrons and ions (mainly protons) which execute quasi-periodic trajectories under the constraining influence of the geomagnetic field [34]. This is the most predictable source of radiation even though it has an stochastic component which depends on the former sources. Hence, this thesis mainly focuses on this kind of radiation to implement the model explained in Chapter 3. Therefore, Section 2.2 only targets this kind of radiation and it analyses the mechanisms by which the trapped particles are governed.

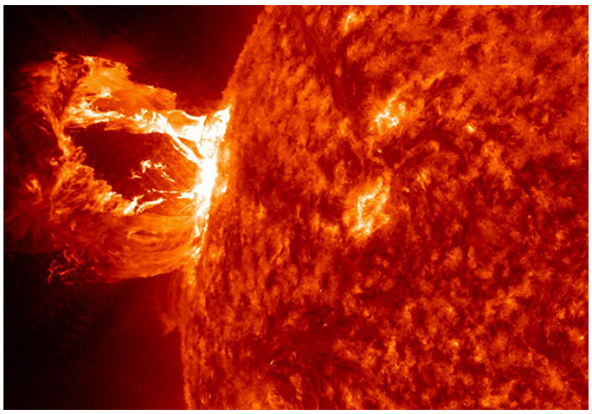

FIGURE 2.1: Solar flare. Image from https://goo.gl/hM7Fk8.

2.2 Van Allen Belts

Even though the Van Allen Radiation Belts were detected for the first time back in 1958, new missions arise nowadays with the purpose of providing new insights about it and its interactions with the Sun. One great example is the NASA's Van Allen Probes mission [35].

The rotation of the Earth's molten iron core results into the creation of electric currents that produce magnetic field lines around the Earth from North to South like a magnet does. The aforementioned magnetic field extends several tens of thousands of kilometers into space, protecting the Earth from the charged particles of the solar wind and cosmic rays that would otherwise strip away the upper atmosphere. A solar wind is a constant stream of particles produced by the Sun, containing a wide range of elements (mainly protons and electrons), and its associated activity varies in intensity with the amount of surface activeness on the Sun. The Earth's magnetosphere shelters the continuous barrage of particles and some of them get trapped in the magnetic field. They give the shape of two toroidal volumes surrounding the Earth called the Van Allen radiation belts, as depicted in Figure 2.2. The inner

belt contains a fairly stable population of protons with energies exceeding 10 MeV (up to 500 MeV). The outer belt contains mainly electrons with energies from 0.04 MeV up to 10 MeV [36].

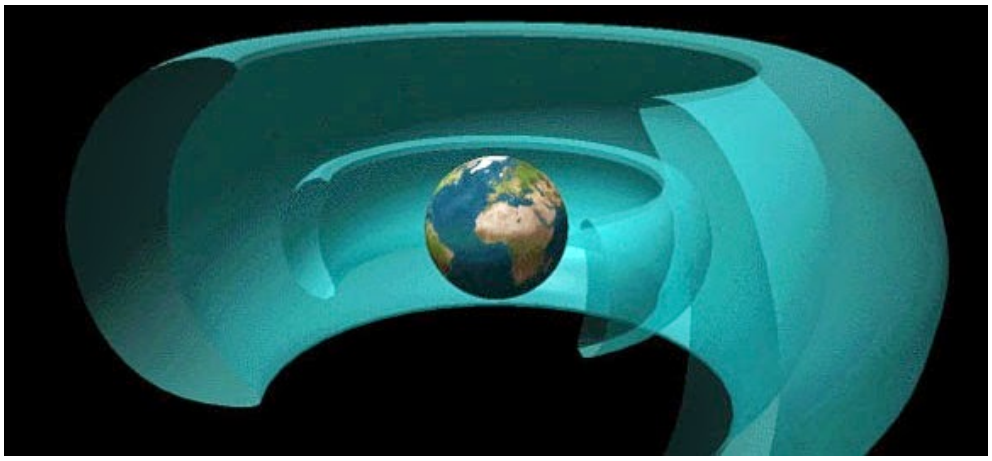

FIGURE 2.2: Simplified representation of Van Allen Belts. Image from https://goo.gl/RKMHAj.

Of special importance for LEO is the so-called South Atlantic Anomaly (SAA), where the fringes of the inner proton radiation belt reach down to altitudes of 200 km over the southern Atlantic Ocean off the coast of Brazil, as depicted in Figure 2.3. This behavior reflects the displacement of the axis of the geomagnetic (dipole) field by about 450 km with respect to the axis of the geoid with a corresponding distortion of the magnetic field. This region accounts for up to 90% of the total exposure in LEO.

The charged particles which compose the belts circulate along the Earth's magnetic lines of force. Their motions are a blend of three periodic motions which take place simultaneously[6]:

- A fast rotation (or "gyration") around magnetic field lines, typically thousands of times each second. Like the motion of planets around the Sun, this motion too can sustain itself with no energy input, and can therefore (in principle) persist for a long time. Opposite charges circle in opposite directions; around a field line pointing towards the viewer, ions circle clockwise, electrons counterclockwise.

- A slower back-and-forth bounce along the field line, typically lasting 1/10 second. As such particles circle their guiding field line, the "guiding center" of their rotation generally slides up or down that line, creating a typical spiral pattern. However, a subtle interaction causes the spiraling particle to be repelled from regions of the stronger magnetic field,

[6] https://www-spof.gsfc.nasa.gov/Education/wtrap1.html last visited on 28th of May, 2018

where field lines converge. This point where the particles are pushed back is called "mirror point".

- In addition to the rapid rotation around field lines and the back-and-forth "bounce" motion, trapped particles also undergo a slow "drift", by which they jump from one field line onto another one nearby, similar to the original one but slightly rotated around the Earth's magnetic axis.

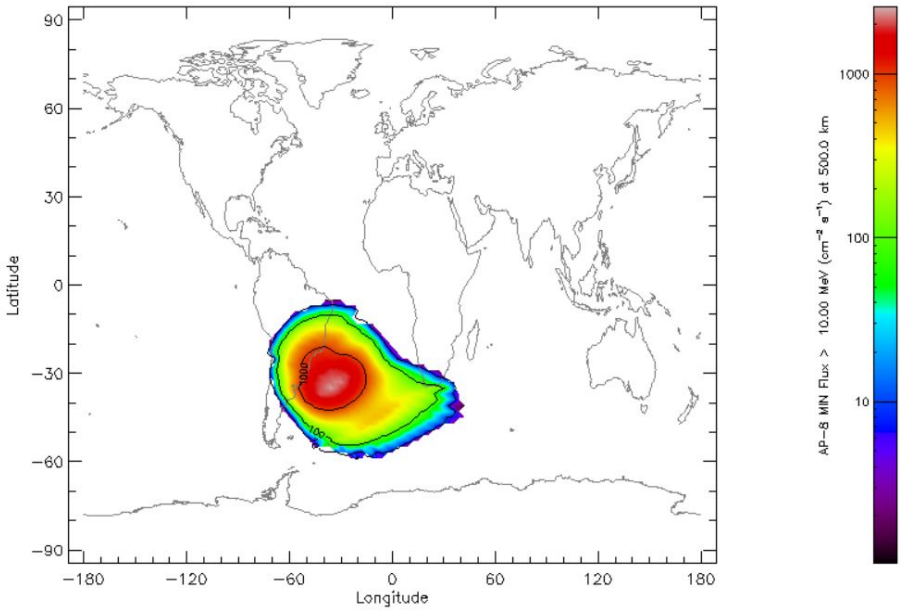

FIGURE 2.3: South Atlantic Anomaly (SAA). Image retrieved from SPENVIS.

The general motion of a particle trapped into the Earth's magnetic field explained above is not simple to imagine. For a better understanding of the reader, this concept is shown in the Figure 2.4.

2.3 Reference Frames

In the following lines, some important reference frames used during this thesis are described and their relations with each other derived.

2.3.1 Geocentric Equatorial Inertial Reference System

The Geocentric Equatorial Inertial Reference System (GEI) has its Z axis parallel to the Earth's rotation axis (positive to the North) and its X axis towards the First Point of Aries (the direction in space defined by the intersection between the Earth's equatorial plane and the plane of its orbit around the Sun (the plane of the ecliptic). This system is (to first order) fixed with respect to

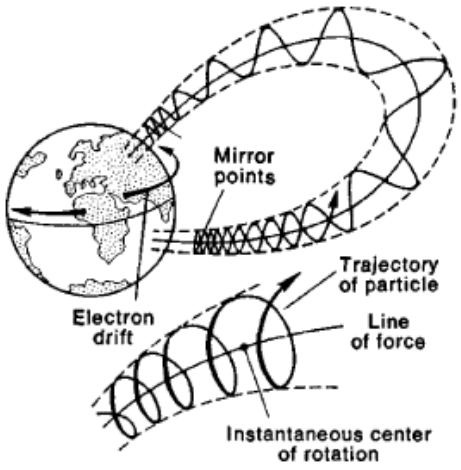

FIGURE 2.4: Motion of charged particles captured in the geomagnetic trap. Image taken from https://www-spof.gsfc.nasa.gov/Education/Iradbelt.html.

the distant stars. It is convenient for specifying the orbits (and hence location) of Earth-orbiting spacecraft as one can specify a Keplerian orbit in this frame. However, note that the GEI system is subject to second-order change with time owing to the various slow motions of the Earth's rotation axis with respect to the fixed stars. Thus for GEI coordinates one must specify the date (normally termed the *epoch*) to which the coordinate system applies. One example is the standard astronomical epoch known as J2000.0, which is 12:00 UT on 1st January 2000. Hence, in this case, a suffix comes along with the acronym of this reference frame, i.e GEI_{2000}.

2.3.2 Geographic Reference System

The Geographic Reference System (GRS) has its Z axis parallel to the Earth's rotation axis (positive to the North) and its X axis towards the intersection of the Equator and the Greenwich Meridian. Thus it is convenient for specifying the location of ground stations and ground-based experiments as these are fixed quantities in the GRS system.

2.3.3 Geomagnetic Reference System

The Geomagnetic Reference System (MAG) gathers capital importance due to the fact that trapped particles follow the Earth's magnetic field lines, as seen in the last Section. As stated in [37], the first approximation for the magnetic field of the Earth is a dipole model. The Geomagnetic Reference System (MAG) has its Z axis parallel to the Earth's magnetic dipole axis (positive North) and its Y axis is the intersection between the Earth's equator and the geographic meridian 90 degrees east of the meridian containing the dipole axis. The X-axis completes the right-hand system.

2.3.4 Coordinate Transformations

Prior to explain the relations and transformation procedures between the reference systems described above, a scheme of them has been depicted in Figure 2.5.

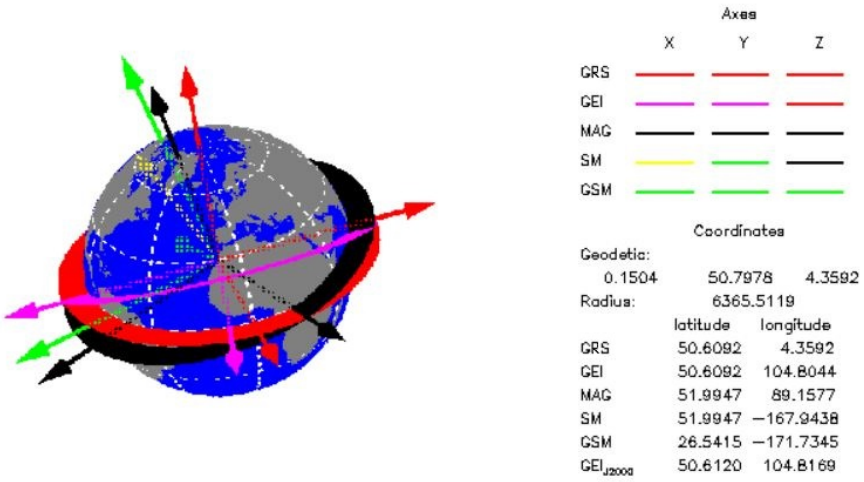

FIGURE 2.5: Coordinate Frames. Retrieved from SPENVIS.

Once the coordinates system have been shown, the transformation procedures are explained. This process has been taken from [38]. The transformations described in the following sections are presented as matrices, which are either a simple rotation matrix (a rotation of angle ζ about one of the principal axes) or are the products of simple rotation matrices. These matrices have only two degrees of freedom and so only two parameters are needed to specify the nine elements in the matrix. These two terms can be the rotation angle and the rotation axis: X, Y or Z, being these three the new axes expressed as unit vectors in the old coordinate system. Thus, a rotation matrix can be specified as

$$\mathbf{E} = \langle \zeta, axis \rangle \tag{2.1}$$

and specify a general product of a matrices as

$$\mathbf{T} = \mathbf{E}_1\mathbf{E}_2 = \langle \zeta_1, axis_1 \rangle \cdot \langle \zeta_2, axis_2 \rangle \tag{2.2}$$

Inversion is straightforward:

$$\mathbf{E}^{-1} = \langle -\zeta, axis \rangle \tag{2.3}$$

$$\mathbf{T}^{-1} = \mathbf{E}_2^{-1}\mathbf{E}_1^{-1} = \langle -\zeta_2, axis_2 \rangle \cdot \langle -\zeta_1, axis_1 \rangle \tag{2.4}$$

Consequently, a rotation of an angle ζ about the Z axis would be expressed in matrix form as [38]

$$\mathbf{E}_3 = \langle \zeta, Z \rangle = \begin{bmatrix} \cos\zeta & \sin\zeta & 0 \\ -\sin\zeta & \cos\zeta & 0 \\ 0 & 0 & 1 \end{bmatrix} \tag{2.5}$$

Analogously, the rotation matrices of angles β and γ about the X and Y axis, respectively read

$$\mathbf{E}_1 = \langle \beta, X \rangle = \begin{bmatrix} 1 & 0 & 0 \\ 0 & \cos\beta & \sin\beta \\ 0 & -\sin\beta & \cos\beta \end{bmatrix} \tag{2.6}$$

$$\mathbf{E}_2 = \langle \gamma, Y \rangle = \begin{bmatrix} \cos\gamma & 0 & \sin\gamma \\ 0 & 1 & 0 \\ -\sin\gamma & 0 & \cos\gamma \end{bmatrix} \tag{2.7}$$

Transformations between three geocentric systems defined above it can be broken down into two fundamental transformations which are described in the following lines. The remaining transformations can then be calculated by matrix operations as shown in Table 2.1.

TABLE 2.1: Breakdown Coordinate Transformations.

	From		
To	GEI	GRS	MAG
GEI	$\mathbf{I}$	$\mathbf{T}_1^{-1}$	$\mathbf{T}_1^{-1}\mathbf{T}_2^{-1}$
GRS	$\mathbf{T}_1$	$\mathbf{I}$	$\mathbf{T}_2^{-1}$
MAG	$\mathbf{T}_2\mathbf{T}_1$	$\mathbf{T}_2$	$\mathbf{I}$

GEI to GRS

$$\mathbf{T}_1 = \langle \theta, Z \rangle \tag{2.8}$$

This matrix corresponds to a rotation in the plane of the Earth's geographic equator from the First Point of Aries to the Greenwich meridian. The rotation angle θ is the Greenwich mean sidereal time. This can be calculated using the following formula [43]

$$\theta = 100.461 + 36000.770T_0 + 15.04107UT \tag{2.9}$$

where

$$T_0 = \frac{MJD - 51544.5}{36525.0} \tag{2.10}$$

with MDJ the Modified Julian Date and UT the universal time.

GRS to MAG

$$\mathbf{T}_2 = \langle \phi - 90^\circ, Y \rangle \cdot \langle \lambda, Z \rangle \tag{2.11}$$

The two rotation are: (i) rotation in the plane of the Earth's equator from the Greenwich meridian to the meridian containing the dipole pole, (ii) rotation in that meridian from the geographic pole to the dipole pole. The angles θ and λ are given by the following equations

$$\lambda = \arctan \frac{h_1^1}{g_1^1} \tag{2.12}$$

$$\phi = 90.0 - \arcsin \frac{g_1^1 \cos\lambda + h_1^1 \sin\lambda}{g_1^0} \tag{2.13}$$

where the values of h_1^1, g_1^1 and g_1^0 are the first order (i.e dipole) coefficients of the International Geomagnetic Reference Field (IGRF), adjusted to the time of interest (geomagnetic field changes continuously).

2.4 Concepts of Interest

In the present Section, some definitions used repeatedly during this document are presented in order to make the reader familiar with them. As stated in [37], the following concepts are referred to particles of a large range of energy E, disregarding their position in space. As explained in Section 2.2, the particles trapped in the belts are constantly moving. Therefore, quantities such as flux or fluence are dependent on the position in which they are measured. In the analysis reported in this thesis, for the sake of simplicity, that spatial dependency has been disregarded. If it was taken into account, then the computation of Van Allen Belts would approximate the reality with a tighter margin of error.

Definition 2. (*Unidirectional Differential Intensity*, $J(E, \theta, \phi, t)$) is the flux [# cm^{-2}][7] of a given energy E per unit energy internal dE in a unit solid angle $d\Omega$ [sr] ($d\Omega = 2\pi \cos\theta d\theta d\phi$) about the direction of observation. The unit of the *Unidirectional Differential Intensity* J is [# $cm^{-2}\ s^{-1}\ sr^{-1}\ keV^{-1}$] for protons and electrons, while it changes for heavy ions (check [17] for more details).

Definition 3. (*Omnidirectional Differential Flux*, $\frac{d\phi(E,t)}{dE}$) of just *Differential Flux* is defined as

$$\frac{d\phi(E,t)}{dE} = \int_{4\pi} J(E, \theta, \phi, t) d\Omega \qquad [\#\ cm^{-2}\ s^{-1}\ keV^{-1}] \tag{2.14}$$

where 4π is the surface of a hypothetical sphere.

[7] the symbol # refers to number of particles

Definition 4. (*Omnidirectional Integral Flux*, $\phi_{\geq E}(t)$ or $\phi(t)$) of just *Integral Flux* is defined as

$$\phi(t) = \int_{E}^{+\infty} \frac{d\phi(E,t)}{dE} dE \qquad [\#\, cm^{-2}\, s^{-1}] \tag{2.15}$$

Definition 5. (*Omnidirectional Differential Fluence*, $\frac{d\Phi(E)}{dE}$) of just *Differential Fluence* is defined as

$$\frac{d\Phi(E)}{dE} = \int_{t_0}^{t_f} \frac{d\phi(E,t)}{dE} dt \qquad [\#\, cm^{-2}\, keV^{-1}] \tag{2.16}$$

Definition 6. (*Omnidirectional Integral Fluence*, $\Phi_{\geq E}$ or Φ) of just *Integral Fluence* is defined as

$$\Phi = \int_{t_0}^{t_f} \int_{E}^{+\infty} \frac{d\phi(E,t)}{dE} dE dt \qquad [\#\, cm^{-2}] \tag{2.17}$$

2.5 Degradation Model of Solar Cells

Solar cell degradation in space is caused primarily by incident protons and electrons either trapped in the Van Allen Belts or ejected in solar events. In planning a space mission, engineers need a method of predicting the expected cell degradation in the space radiation environment. This is not a simple calculation, however, because the rate of degradation for a given type of cell depends on the energies of the incident protons and electrons. In addition, the front surface of the cell is usually shielded by coverglass, and the back surface by the substrate material of the cell and the supporting array structure, so that the incident particle spectrum is "slowed down" before it impinges on the active regions of the cell. Finally, different kinds of cell technologies respond differently to irradiation depending on the materials used, the thickness of the active regions, and the types and concentrations of dopants employed [39]. For this analysis, silicon solar cells have been reported.

A solar cell it is basically characterized by three parameters: maximum power (P_{max}), open circuit voltage (V_{oc}) and cell short circuit intensity (I_{sc}). A generic current-voltage curve for a solar cell has been represented in Figure 2.6 when it comes to silicon solar cells. In this thesis, the degradation model of solar cells has been taken essentially as a tool in order to build the model extensively explained in the next Chapter. Therefore, only the Equivalent Fluence Theory (EFT), developed by JPL [39], is properly explained in this Section. For further details about solar cell degradation models, the reader is referred to [37, 39].

Although the definitions provided in the last Section are correct, the solar cell degradation effect has not been taken into account. Therefore, in the following lines, it is explained how those formulas vary when this phenomenon is added. This variation arises as a result of the Equivalent Fluence Theory, which is explained below. First of all it is necessary to remark that in this theory, the monoenergetic particle of 1 MeV electron is taken as a reference. The reason for this decision are few but it especially matters the fact that it is a significant component in space radiation and it can be produced conveniently in a test environment [39]. As a result, 1 MeV electron fluence (Φ_e^{1MeV}) remains as the damage equivalent fluences which describe silicon solar cell degradation. For the case of protons, on the other hand, this damage is quantified at 10 MeV. For this reason, the proton damage ratio must be scaled in order to have an equivalent damage at a certain energy (1 MeV), a fact that gives the name to this theory. The EFT uses this idea to assess the solar cell performance during a generic space transfer.

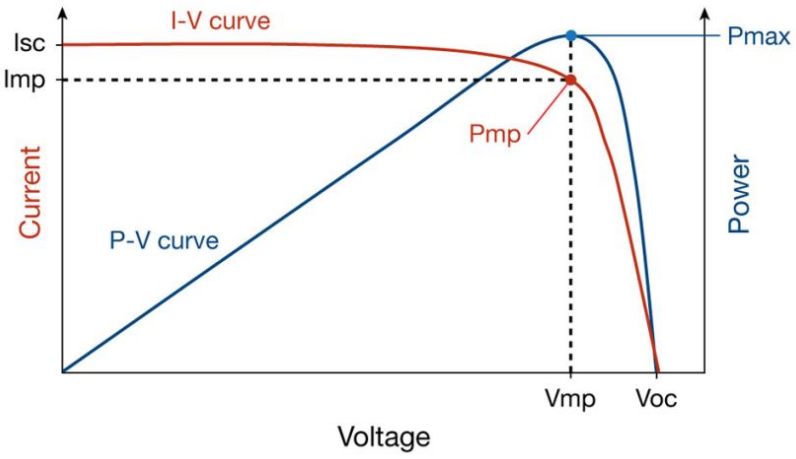

FIGURE 2.6: Current-Voltage curve. Retrieved from [37].

The Relative Damage Coefficient (RDC), $D_{e,p}(E,\kappa)$, is a factor which represents the damage ratio in the cell: it depends on the energy level, E, and the coverglass thickness, κ. Obviously, this coefficient is different for protons/electrons and it also changes with the solar cell. Moreover, RDC values depend on the operational mode of the photovoltaic (P_{max}, V_{oc} or I_{sc}). Hence, the evaluation of the equivalent fluences for electrons/protons yields

$$\Phi_e^{1MeV} = \int_{E_e}^{\infty} \frac{d\Phi_e(E)}{dE} \cdot D_e(E,\kappa) dE \tag{2.18}$$

$$\Phi_p^{10MeV} = \int_{E_p}^{\infty} \frac{d\Phi_p(E)}{dE} \cdot D_p(E,\kappa) dE \tag{2.19}$$

where the subindexes e and p stand for electrons and protons, respectively. Analogously, E_e^{min} is the minimum energy selected for the electron fluence integration while E_p^{min} is the one for protons. In order to have the equivalent fluences, as commented before, it is needed to have both quantities at the same energy level. Thus, a conversion parameter (α_{p-e}) has been defined for the proton equivalent fluence, which transforms the 10 MeV proton fluence to the fluence that 1 MeV electrons would have.

$$\Phi_p^{1MeV} = \alpha_{p-e} \cdot \Phi_p^{10MeV} \tag{2.20}$$

The *total equivalent fluence*, hence, is computed as follows

$$\Phi_{total}^{1MeV} = \Phi_e^{1MeV} + \Phi_p^{1MeV} \tag{2.21}$$

This quantity is a key feature of this thesis. As it will be explained in detail later, it is the one which will be minimized while calculating the radiation optimal trajectory. In order to set down some considerations and translate the last few paragraphs into numbers, the Spectrolab XTJ solar cell has been selected regarding this work, whose conversion parameters are shown in Table 2.2.

TABLE 2.2: Spectrolab XTJ Conversion Parameters.

Parameter	α_{e-p}
P_{max}	830
V_{op}	782
I_{sc}	442

Moreover, it has been considered that the photovoltaic is working at P_{max} conditions for the calculations carried out during this research. Therefore, $\alpha_{e-p} = 830$.

Chapter 3

Flux Distribution Model of Van Allen Belts

"If you want to find the secrets of the universe think in terms of energy, frequency and vibration"

- Nikola Tesla, *1856 - 1943*

SHORTLY after its discovery in 1958, the radiation belts became one of the most intriguing goals to pursue, not only in order to understand but model them in a faithful manner. The main difficulty lies in the fact that the undergoing processes which characterize them are highly stochastic. For instance, they are strongly dependent on solar cycles and solar activity, being this latter another stochastic process itself. Therefore, the closest approach to represent their behavior is through statistical methods. It can be done by gathering huge amount of data throughout the appropriate instruments aboard suitable satellites. This collected database is processed, analyzed, coded and, as a result, different radiation models are developed. The latest one released has been the AE9/AP9/SPM, or International Radiation Environment Near Earth (IRENE) [17], as the predecessor of the AE8/AP8/SPM. The main improvements regarding the last version (version 9) include a narrower spatial grid and the quantification of uncertainty due to both space weather and instrument errors [44].

3.1 Goals of the Model

The radiation model developed throughout this thesis is explained throughout this Chapter and it has straightforward goals. Firstly, it comes motivated by the need of a method to measure the radiation flux generated by electrons and protons encapsulated in the Van Allen belts while performing a general transfer in Earth centered environments. When the model was first

conceived, another requisite was to develop it in an efficient manner in order to get fast and robust outputs. Simultaneously, it had to be simple. This comes as a high-level requirement to achieve a solution of compromise between computational time and trustworthy results. The reason behind it lies in the fact that the present model will be integrated into a solver developed at Politecnico di Milano to compute radiation optimal trajectories minimizing the radiation which encounters the satellite through its transfer path. The indirect approach has been applied to solve the optimization problem. This method may need large computation times, so the fact of developing the radiation module as simple as possible but in a consistent and robust way is a priority.

3.2 Assumptions and Simplifications

This Section provides the reader an overview of the main assumptions and simplifications done during the development of this model. In fact, these suppositions will drive most of the shortages listed in Section 4.7 because they fundamentally are unavoidable consequences.

The first and the strongest assumption which has been taken into account is the two-dimensional frame in which the model has been established. Even though the design process will be fully detailed in Section 3.3, it can be said in advance that the spatial grid used was projected onto the equatorial plane, i.e. orbital inclination equal to zero. Therefore, due to the strategy used for mapping the differential fluxes explained in the next Section, this model results to be symmetrical around latitude and longitude. Thus, for the sake of simplicity, and owing to the fact that the spacecraft's instantaneous position vector provided by the solver comes in GEI coordinates as well, the present radiation model has been computed in the same reference system. Despite the fact that the current model could be perfectly suitable for three-dimensional frame (like the aforementioned solver), it will be only accurate as long as the Z coordinate remains close to zero.

Softer but not less important considerations have been included. One of them comprehends the epoch selected for the computation of the built-up model. An iterative analysis has been done to decide on this matter. As commented before, solar cycles affects the behavior of the Van Allen belts. Consequently, some comparisons are needed to pick a certain epoch accordingly. In Figure 3.1, where the limits for proton energies $E_p \in [0.1, 200]$ MeV and altitudes from $h \in [200, 60000]$ km. The analysis has been computed through AE9/AP9/SPM tool. It has only been represented for the protons since that is the main source of radiation in terms of flux. The tights differences shown in

that Figure justify some freedom margin to select the aforementioned epoch. In this thesis, it has been chosen as the 1st January of 2018, 00:00:00 UT.

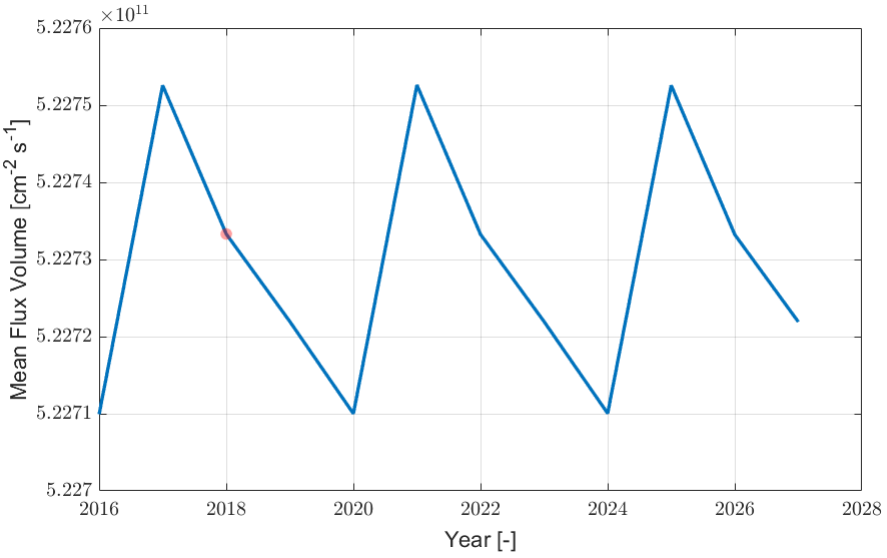

FIGURE 3.1: Proton averaged volume flux comparison over 11-years solar cycle.

Another consideration which has a great impact on the results is the model of solar cell which has been used (see Section 2.5). Provided by SPENVIS, it maps the RDC as a piece-wise heaviside function instead of as a continuous one. RDC function for protons has been depicted in Figure 3.2 for diverse coverglass thicknesses. Its limits in energy have been shorten in the Figure to be able to see the heavyside behavior, even though this functions map the entire energy spectrum commented previously. It is straightforward to figure the approximation errors adjoined to this case. Anyhow, it has been kept in this form due to the flexibility it grants when variations of the coverglass thickness parameter are needed.

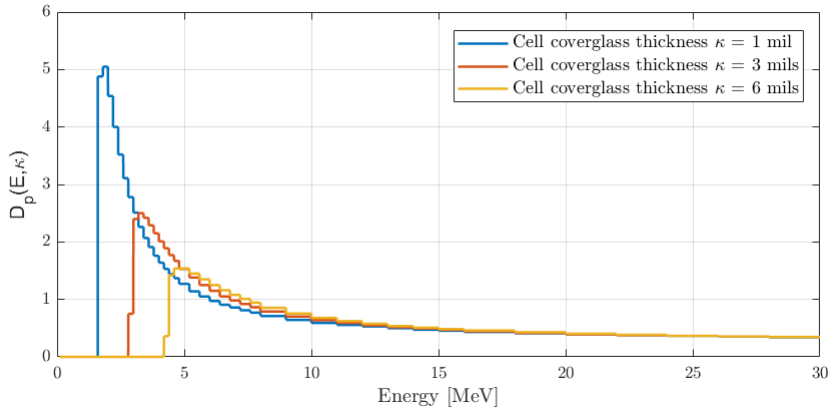

FIGURE 3.2: Proton RDC function.

3.3 Computational Design Strategy

Previous to explain the model's baseline design, it is mandatory to go through some basic IRENE's concepts. One of them is the diversity of run modes that AE9/AP9/SPM tool includes. It is of capital importance to understand what does each run mode account for and which one is the most suitable for a certain analysis. These run modes are [17]:

- **Mean or Percentile:** Mean mode provides a quick estimate of the environment and effects. Percentile mode is appropriate only for comparing with measurements at a given location and energy. The internal model flux map behavior remains static throughout the run, while the value initialization is either the mean or percentile. The output of this run mode is the mean or selected percentile.

- **Perturbed Mean:** this run mode is appropriate for cumulative/integrated quantities such as fluence, for instance. The internal model flux map behavior remains static throughout the run, while the value initialization accounts for the mean values with random perturbations for each scenario. Its outputs are confidence intervals based on model uncertainties depending on the number of scenarios analyzed.

- **Monte Carlo:** it provides an estimate of uncertainty in time-varying quantities. The internal model flux map behavior evolves as time progresses while its initialization values are the mean values with random perturbations for each scenario. Its outputs are confidence intervals including space weather based on the number of scenarios analyzed.

Regarding the type of computations needed for the model under construction (flux and fluences), the perturbed run mode with 100 scenarios has been used. It has been considered the 95^{th} percentile as aggregation mode. The logic which has been followed to build the radiation model under study is summarized in Figure 3.3 and its processes are explained in the successive lines.

The first process comprehends the initialization of the main parameters of interest. These are the following:

- Vector of altitudes **h**. Ranging from 200 km to 60000 km with a step size of $\delta = 39.86$ km, or in a general way, N discretizations.

- Electron and proton vectors, $\mathbf{E_e}$ and $\mathbf{E_p}$ with a generic number of components M, same for both. Their limits are $E_e = 0.04 - 10$ MeV and $E_p = 0.1 - 200$ MeV, respectively. It is important to notice that plasma has not been included in this analysis (particles below 0.04 MeV energy

levels) due to the fact that these particles do not contribute to a remarkable solar cell degradation [48].

- The Julian days during which the ephemeris at the h_k altitude is run, J_d. In this work, 92 Julian days have been considered for all the iterations starting from the 1st of January 2018.
- Right Ascension of Ascending Node (RAAN), the argument of perigee, the true anomaly at the departure, inclination, and eccentricity are all equal to zero. Thus, all the ephemeris are contained in the equatorial plane and they are circular orbits.

The parameter k in the Figure 3.3 simulates the *for* loop in the code. Hence, in this very case, $k = 1, 2, ..., N$, being $N = 1500$. After the initialization of the parameters, with an altitude h_k defined already, the circular trajectory during 92 Julian days is calculated and a .txt file is generated in the suitable format for the posterior analysis through IRENE models.

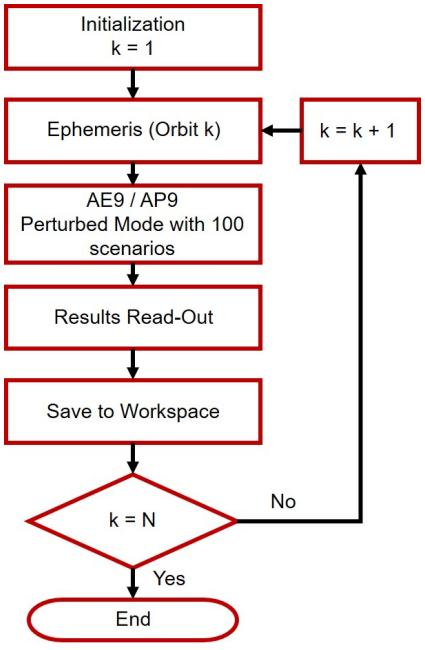

FIGURE 3.3: Design strategy flowchart.

In order to implement the ephemeris, the basic equations of orbital mechanics have been coded. One essential remark comes motivated by the sample times, which are dependent on the altitude. In accordance to [49], the recommended (and utilized) ones are shown in Table 3.1, where $R_E = 6378$ km is the Earth's radius.

Once the .txt file with the ephemeris has been created, it is sent to the AE9 and AP9 modules, in which it is analyzed and the results written into .txt files. It is noteworthy to keep in mind the type of analysis done at this point. Both

modules are run at *perturbed mode* with 100 scenarios while 95th percentile is considered. Once the differential flux is calculated for both electrons and protons, the average value over the entire trajectory (92 days) is taken as the

TABLE 3.1: Recommended Sample Times.

Interval	Sample Time [s]
$h_k \leq 1.3R_E$	10
$1.3R_E < h_k \leq 2R_E$	60
$2R_E < h_k \leq 4R_E$	300
$h_k > 4R_E$	900

final output. These values of the differential fluxes are computed for every energy level predefined by E_p and E_e, respectively. Therefore, they are vectors with the same number of components that the aforementioned energy vectors (M components). These vectors are the responsible ones of filling the differential flux surfaces saved in the workspace gradually as matrices: $\mathbf{F_p}$ for protons and $\mathbf{F_e}$ for electrons. In a mathematical way, this yields

$$\mathbf{F_p}(1:M,k) = \frac{d\phi_p(E_p,h_k)}{dE_p} \tag{3.1}$$

$$\mathbf{F_e}(1:M,k) = \frac{d\phi_e(E_e,h_k)}{dE_e} \tag{3.2}$$

In the Figures 3.4, the result of the detailed process described above is given. As the reader could notice, these graphs are in linear scale and they are quite steep for low energy levels, a fact that could be a major difficulty to interpolate them.

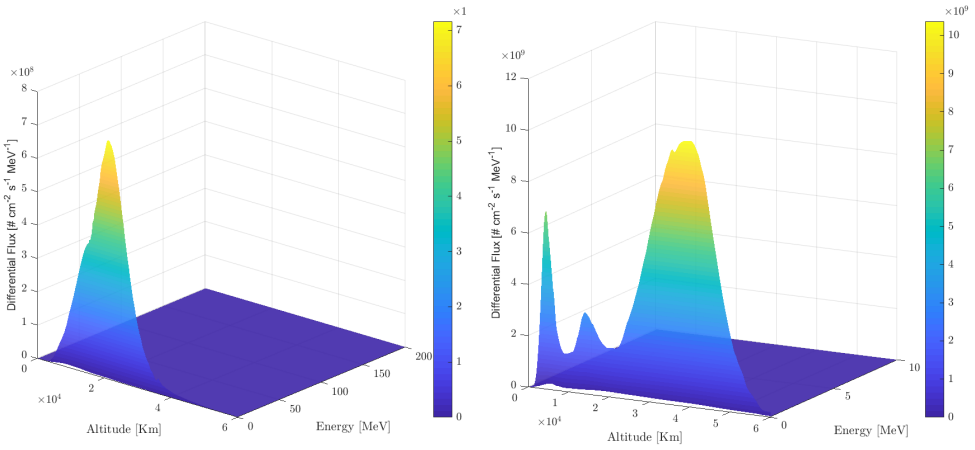

FIGURE 3.4: Linear differential flux distribution for protons (left) and electrons (right).

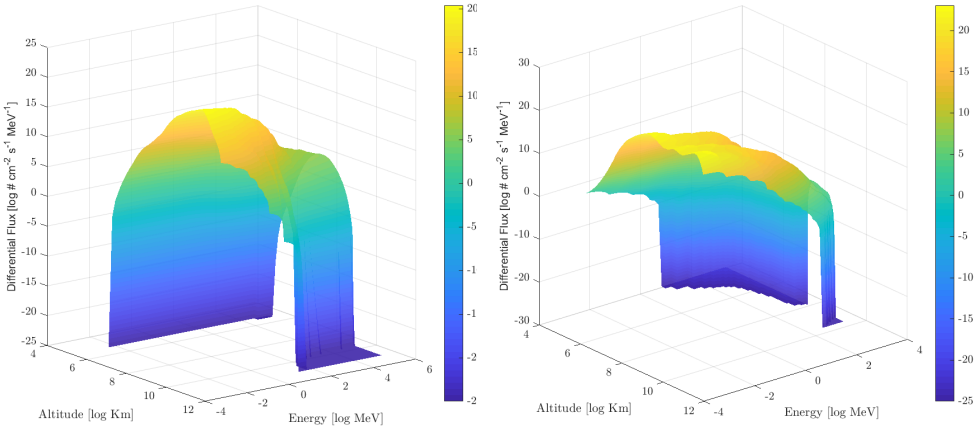

FIGURE 3.5: Logarithmic differential flux distribution for protons (left) and electrons (right).

For facing this problem, they have been finally represented in logarithmic scale, as shown in the Figures 3.5. Then, they have been approximated through a linear interpolation and saved afterward into two structure variables, one for each particle type. To finalize the current Section, both 2-D integral flux models for protons and electrons have been depicted in Figure 3.6. As can be seen in the Figures and according to [17], the inner belt extends from approximately hundreds of kilometers to 6000 km in altitude and is populated by high energy protons and medium energy electrons, while the outer belt, up to 60,000 km in altitude, is predominately populated by electrons.

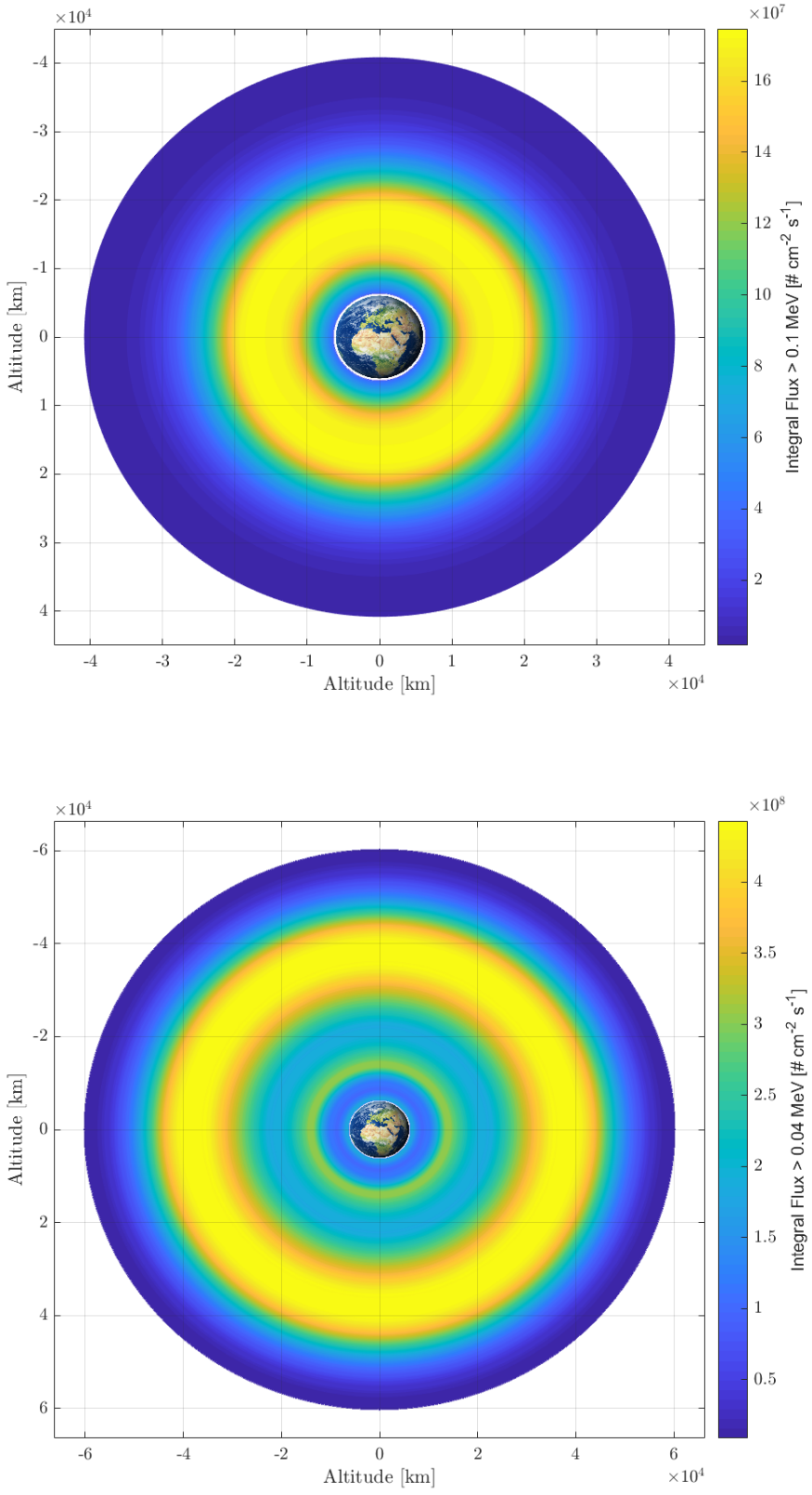

FIGURE 3.6: 2-D Model of Van Allen Belts for protons (top) and electrons (bottom) in GEI reference frame.

Chapter 4

Low Thrust Radiation Optimal Trajectory Problem

"Human knowledge is personal and responsible, an unending adventure at the edge of uncertainty"

- Jacob Bronowski, *1908 - 1974*

INCIDENT radiation contribution of Van Allen Belts generates significant failures within the satellite, especially in solar cells through degradation processes. Regarding this fact, reducing spacecraft's radiation exposure is a major challenge. In this Chapter, the low-thrust transfer to GEO with fix TOF has been investigated. The main aim in this approach consists in minimizing the total equivalent fluence while the spacecraft is flying across the Van Allen Belts. The problem has been framed and analyzed using the indirect method.

4.1 Dynamic Model

Prior to formulating optimal trajectory problem, it is mandatory to set the dynamics equations which model the spacecraft. These equations are affected by the Earth gravitational acceleration and the thrust provided by the spacecraft itself, which is considered as a point mass body. As known from the literature, Kepler's problem is a particular case derived from the two-body problem in which they interact by means of a central force. The spacecraft's dynamics in an inertial reference frame is formulated in Cartesian coordinates as follows

$$\frac{d^2\mathbf{r}}{dt^2} = -\mu\frac{\mathbf{r}}{|\mathbf{r}|^3} + \frac{\mathbf{T}}{m} \tag{4.1}$$

where $\mathbf{r} \in \mathbb{R}^3$ represents the position vector, $\mathbf{T} \in \mathbb{R}^3$ stands for the thrust vector, m is the spacecraft's mass and $\mu = G \cdot M_E$ is the Earth gravitational

constant, with G the universal gravitational constant and M_E the mass of the Earth.

The final purpose of this thesis consist in integrating the aforementioned equation over time, restricting initial and final positions and velocities, for a given initial mass of the spacecraft. When low-thrust propulsion is considered, it is convenient to express the equations of motion in nondimensional space state form as [7]:

$$\dot{\mathbf{x}} = \mathbf{f}(\mathbf{x}, \boldsymbol{\alpha}, u) \Rightarrow \begin{bmatrix} \dot{\mathbf{r}} \\ \dot{\mathbf{v}} \\ \dot{m} \end{bmatrix} = \begin{bmatrix} \mathbf{v} \\ \mathbf{g}(\mathbf{r}) + uT_{max}\boldsymbol{\alpha}/m \\ -uT_{max}/c \end{bmatrix} \tag{4.2}$$

where $\mathbf{r} = [x, y, z]^\top$ is the position vector as commented before, $\mathbf{v} = [v_x, v_y, v_z]^\top$ denotes the spacecraft velocity vector, T_{max} represents the maximum thrust magnitude and $c = I_{sp}g_0$ is the exhaust velocity, with I_{sp} the thruster specific impulse and g_0 the gravitational acceleration at sea level. The control variables are the throttle factor, $u \in [0, 1]$, and the thrust direction unit vector $\boldsymbol{\alpha}$. The function $\mathbf{g}(\mathbf{r})$ is defined as, according to the two body problem

$$\mathbf{g}(\mathbf{r}) = \begin{bmatrix} -\mu \frac{x}{|\mathbf{r}|^3} \\ -\mu \frac{y}{|\mathbf{r}|^3} \\ -\mu \frac{z}{|\mathbf{r}|^3} \end{bmatrix} \tag{4.3}$$

The boundary conditions correspond to two given states; a initial point $(\mathbf{r}_i, \mathbf{v}_i)$, and a final point $(\mathbf{r}_f, \mathbf{v}_f)$. Hence, the boundary conditions yield

$$\begin{aligned} \mathbf{r}(t_i) - \mathbf{r}_i = 0, \qquad & \mathbf{v}(t_i) - \mathbf{v}_i = 0, \\ \mathbf{r}(t_f) - \mathbf{r}_f = 0, \qquad & \mathbf{v}(t_f) - \mathbf{v}_f = 0, \\ m(t_i) - 1 = 0 & \end{aligned} \tag{4.4}$$

where the initial mass has been scaled to one. On the other hand, the final mass is unconstrained.

4.2 Optimal Control Theory

As stated at the beginning of this Chapter, the indirect method has been used to solve the optimal transfer problem described hereinafter. The indirect methods are based on the Calculus of Variations and the Pontryagin's Minimum Principle [45, 46]. Even though the dynamics of the system regarding this work has been already described, in this Section a general dynamics

have been taken into account in order to generalize the optimal problem under study. This summary has been taken from [6]. First of all, the general form to describe the dynamics of the system is

$$\dot{\mathbf{x}} = \mathbf{f}(\mathbf{x}(t), \mathbf{u}(t), t) \quad \text{with} \quad \mathbf{x}(t_0) = \bar{\mathbf{x}}_0, \qquad t_0 \leq t \leq t_f \tag{4.5}$$

where, for the general case, $\dot{\mathbf{x}}(t) \in \mathbb{R}^n$ is the state vector and $\mathbf{u}(t) \in \mathbb{R}^m$ is the control vector. Quite generally, there are some components of the state vector which are constrained at their final time in order to comply with the requirements of the mission. These constraints are represented by the terminal function $\boldsymbol{\Psi}(\mathbf{x}_f, t_f) = \mathbf{0}$, where $\boldsymbol{\Psi} \in \mathbb{R}^q$ with $q \leq n$. The next logical step becomes to define the scalar performance index J, which can be expressed in the Bolza form as

$$J = \boldsymbol{\Theta}(\mathbf{x}(t_f), t_f) + \int_{t_0}^{t_f} L(\mathbf{x}(t), \mathbf{u}(t), t)dt \tag{4.6}$$

where J is called functional because it transforms functions into numbers, i.e. the state vector or the control vector. The term inside the integral is called *Lagrangian* and it denotes the cost function to be minimized during the transfer. On the other hand, the term $\boldsymbol{\Theta}$ includes both a terminal cost function $\theta(\mathbf{x}(t_f), t_f)$ and the constraints in the final state $\boldsymbol{\Psi}$. The latter term must be multiplied by a constant Lagrange vector $\boldsymbol{\nu} \in \mathbb{R}^q$.

$$\boldsymbol{\Theta}(\mathbf{x}(t_f), t_f) = \theta(\mathbf{x}(t_f), t_f) + \boldsymbol{\nu}^\top \boldsymbol{\Psi}(\mathbf{x}_f, t_f) \tag{4.7}$$

In the case that $\boldsymbol{\Theta}$ can be differentiated, the equation above can be expressed as [40]

$$\boldsymbol{\Theta}(\mathbf{x}(t_f), t_f) = \boldsymbol{\Theta}(\mathbf{x}(t_0), t_0) + \int_{t_0}^{t_f} \frac{d\boldsymbol{\Theta}(\mathbf{x}(t), t)}{dt} dt \tag{4.8}$$

Therefore, the performance index expression yields

$$J = \boldsymbol{\Theta}(\mathbf{x}(t_0), t_0) + \int_{t_0}^{t_f} [L(\mathbf{x}(t), \mathbf{u}(t), t) + \frac{d\boldsymbol{\Theta}(\mathbf{x}(t), t)}{dt}]dt \tag{4.9}$$

Since $\mathbf{x}(t_0)$ and t_0 are fixed, the minimization process does not affect the $\boldsymbol{\Theta}(\mathbf{x}(t_0), t_0)$, which represents an offset. Using the chain rule of differentiation, it is found that the performance index J becomes

$$J = \int_{t_0}^{t_f} [L(\mathbf{x}(t), \mathbf{u}(t), t) + \left[\frac{\partial \boldsymbol{\Theta}(\mathbf{x}(t), t)}{\partial \mathbf{x}}\right]^\top \dot{\mathbf{x}}(t) + \frac{\partial \boldsymbol{\Theta}(\mathbf{x}(t), t)}{\partial \mathbf{x}}]dt \tag{4.10}$$

Hence, the optimization problem consists in finding a $\mathbf{u}^*(t)$ such as the functional J is minimized. To include the dynamics of the problem, it is needed to add the differential set of equations (Eq. (4.5)) by time-dependent Lagrange

multipliers $\boldsymbol{\lambda}(t) \in \mathbb{R}^n$. In order to do that, an augmented performance index $\tilde{J}$ is presented

$$\begin{aligned}\tilde{J} = \int_{t_0}^{t_f} L(\mathbf{x}(t), \mathbf{u}(t), t)dt + \int_{t_0}^{t_f} \left[\frac{\partial \boldsymbol{\Theta}(\mathbf{x}(t), t)}{\partial \mathbf{x}}\right]^\top \dot{\mathbf{x}}(t)dt + \\ + \int_{t_0}^{t_f} \left[\frac{\partial \boldsymbol{\Theta}(\mathbf{x}(t), t)}{\partial \mathbf{x}} + \boldsymbol{\lambda}^\top(t)[\mathbf{f}(\mathbf{x}(t), \mathbf{u}(t), t) - \dot{\mathbf{x}}]\right] dt\end{aligned} \tag{4.11}$$

by redefining the Lagrangian

$$\begin{aligned}\tilde{L}(\mathbf{x}(t), \dot{\mathbf{x}}(t), \mathbf{u}(t), \boldsymbol{\lambda}(t), t) = L(\mathbf{x}(t), \mathbf{u}(t), t) + \left[\frac{\partial \boldsymbol{\Theta}(\mathbf{x}(t), t)}{\partial \mathbf{x}}\right]^\top \dot{\mathbf{x}}(t) + \\ + \frac{\partial \boldsymbol{\Theta}(\mathbf{x}(t), t)}{\partial \mathbf{x}} + \boldsymbol{\lambda}^\top(t)[\mathbf{f}(\mathbf{x}(t), \mathbf{u}(t), t) - \dot{\mathbf{x}}]\end{aligned} \tag{4.12}$$

the optimization problem can be derived. The necessary conditions of $\tilde{J}$ to be an extreme are computed by setting the total variation $\delta\tilde{J}$ equal to zero. As a consequence, the variations $\delta\mathbf{x}$, $\delta\dot{\mathbf{x}}$, $\delta\mathbf{u}$, $\delta\boldsymbol{\lambda}$ and δt_f are introduced.

$$\begin{aligned}\delta\tilde{J} = 0 = \left[\frac{\partial \tilde{L}}{\partial \dot{\mathbf{x}}}\right]_{t=t_f} \delta\mathbf{x}_f + \left[\tilde{L}(t_f) - \left[\frac{\partial \tilde{L}}{\partial \dot{\mathbf{x}}}\right]_{t=t_f} \dot{\mathbf{x}}(t_f)\right] \delta t_f + \\ + \int_{t_0}^{t_f} \left[\left(\frac{\partial \tilde{L}}{\partial \mathbf{x}} - \frac{d}{dt}\frac{\tilde{L}}{\partial \dot{\mathbf{x}}}\right) \delta\mathbf{x}(t) + \frac{\partial \tilde{L}}{\partial \mathbf{u}}\delta\mathbf{u}(t) + \frac{\partial \tilde{L}}{\partial \boldsymbol{\lambda}}\delta\boldsymbol{\lambda}(t)\right] dt\end{aligned} \tag{4.13}$$

It has been assumed that the second partial derivatives are continuous. As a result, the order of differentiation can be interchanged. As known from the literature, integral terms yield to equations and boundary terms result as conditions. When the expression of L is introduced into the last equation, the integral term reads

$$\begin{aligned}\int_{t_0}^{t_f} \left(\frac{\partial L}{\partial \mathbf{x}} + \boldsymbol{\lambda}(t)\frac{\partial \mathbf{f}}{\partial \mathbf{x}} + \frac{d}{dt}\boldsymbol{\lambda}(t)\right) \delta\mathbf{x}(t) + \\ \left(\frac{\partial L}{\partial \mathbf{u}} + \boldsymbol{\lambda}(t)\frac{\partial \mathbf{f}}{\partial \mathbf{u}}\right) \delta\mathbf{u}(t) + \\ + (\mathbf{f} - \dot{\mathbf{x}}(t))\delta\boldsymbol{\lambda}(t)dt\end{aligned} \tag{4.14}$$

In order to guarantee the extreme condition, the whole integral must vanish regardless of the boundary conditions. If the *Hamiltonian* is defined as

$$H(\mathbf{x}(t), \mathbf{u}(t), t) = L(\mathbf{x}(t), \mathbf{u}(t), t) + \boldsymbol{\lambda}^\top(t)\mathbf{f}(\mathbf{x}(t), \mathbf{u}(t), t) \tag{4.15}$$

consequently, the constraints from Equation (4.13) are

$$f(x) = \begin{cases} \dot{\mathbf{x}} = \mathbf{f}(\mathbf{x}^*(t), \mathbf{u}^*(t), t) = \frac{\partial H}{\partial \boldsymbol{\lambda}} \\ \dot{\boldsymbol{\lambda}} = -\frac{\partial H}{\partial \mathbf{x}} \\ \frac{\partial H}{\partial \mathbf{u}} = \mathbf{0} \end{cases} \tag{4.16}$$

resulting the set (4.16) in the *Euler-Lagrange equations*, which are the basis of COV. Taking now the non integral terms of Equation (4.13) and making them zero

$$\left[\frac{\partial \boldsymbol{\Theta}(\mathbf{x}^*(t_f), t_f)}{\partial \mathbf{x}} - \boldsymbol{\lambda}(t_f)\right] \delta \mathbf{x}_f + \left[H(t_f) + \frac{\partial \boldsymbol{\Theta}(\mathbf{x}^*(t_f), t_f)}{\partial t}\right] \delta t_f = 0 \tag{4.17}$$

equality which gives rise to the terminal conditions

$$H(t_f) = -\frac{\partial \boldsymbol{\Theta}(\mathbf{x}^*(t_f), t_f)}{\partial t} \tag{4.18}$$

$$\boldsymbol{\lambda}(t_f) = \frac{\partial \boldsymbol{\Theta}(\mathbf{x}^*(t_f), t_f)}{\partial \mathbf{x}} \tag{4.19}$$

It is of capital importance to notice that there is still one condition to apply regarding the last equation of (4.16). This condition represents the constrained control. In order to do that, the Pontryagin's Minimum Principle [50] must be applied. The PMP states that the bounded control $\mathbf{u}^*(t)$ is computed by a local optimization of the Hamiltonian at every single time step. Considering the fact that $0 \leq |\mathbf{u}| \leq 1$, the PMP reads

$$H(\mathbf{x}^*(t), \mathbf{u}^*(t), \boldsymbol{\lambda}(t), t) \leq H(\mathbf{x}^*(t), \mathbf{u}(t), \boldsymbol{\lambda}(t), t) \tag{4.20}$$

which means that an admissible control must ensure that the Hamiltonian takes its minimum value

$$\mathbf{u}(t) = \text{argmin}_{\mathbf{u}} H(\mathbf{x}(t), \mathbf{u}(t), \boldsymbol{\lambda}(t), t) \tag{4.21}$$

At this point, once the problem has been stated in *Euler-Lagrange* form and its adjoined boundary conditions regarding the augmented system $\mathbf{y} = [\mathbf{x}, \boldsymbol{\lambda}]^\top$ can be divided into initial and final constraints, as shown as follows, the problem under consideration becomes a *Two Point Boundary Value Problem* (TPBVP).

$$\mathbf{x}(t_0) = \bar{\mathbf{x}}_0 \tag{4.22}$$

$$\boldsymbol{\lambda}(t_f) = \frac{\partial \boldsymbol{\Theta}(\mathbf{x}^*(t_f), t_f)}{\partial \mathbf{x}} \tag{4.23}$$

$$\boldsymbol{\Psi}(\mathbf{x}^*(t_f), t_f) = \mathbf{0} \tag{4.24}$$

4.3 Radiation Optimal Transfer Problem

Once the general formulation of the optimal problem has been presented, it has been particularized for the case of radiation optimal transfer. All the variables of interest such as states, costates and control vector have been arranged

accordingly with the features of the current problem under study. Firstly, the augmented performance index $\tilde{J}$ is defined as

$$\begin{aligned}\tilde{J} &= \Theta + \int_0^{t_f} [L + \boldsymbol{\lambda}^\top (\mathbf{f} - \dot{\mathbf{x}})] dt \\ &= \Theta + \int_0^{t_f} [H + \boldsymbol{\lambda}^\top \dot{\mathbf{x}}] dt\end{aligned} \tag{4.25}$$

$$\mathbf{x} = [\mathbf{r}, \mathbf{v}, m]^\top \in \mathbb{R}^7 \tag{4.26}$$

$$\boldsymbol{\lambda} = [\boldsymbol{\lambda}_r, \boldsymbol{\lambda}_v, \lambda_m]^\top \in \mathbb{R}^7 \tag{4.27}$$

$$H = \boldsymbol{\lambda}_r \cdot \mathbf{v} + \boldsymbol{\lambda}_v \cdot (\mathbf{g}(\mathbf{r}) + u T_{max} \boldsymbol{\alpha} / m) - \lambda_m \cdot u T_{max} / c + L \tag{4.28}$$

Throughout this procedure, the variables' dependencies have been neglected to make the process clearer to the reader. The initial time has been set to zero. Since the main challenge of this thesis consists on minimizing the total equivalent fluence at 1 MeV, the functional J reads

$$J = \int_0^{t_f} L dt = \int_0^{t_f} G_r dt \tag{4.29}$$

where

$$G_r = \int_{E_0}^{E_f} \left[\frac{d\phi_p(h,E)}{dE} \cdot D_p(E,\kappa) \cdot \alpha_{p-e} + \frac{d\phi_e(h,E)}{dE} \cdot D_e(E,\kappa) \right] dE \tag{4.30}$$

stands for the total equivalent flux at 1 MeV, according to the nomenclature presented in Chapter 2, where κ accounts for the coverglass thickness of the solar cell. It is important to remark that, the differential fluxes in the last equation do not depend anymore on time but on the altitude once the spatial grid explained in Chapter 3 has been utilized to model the Van Allen belts. Therefore, the dynamics for the costates is governed by

$$\dot{\boldsymbol{\lambda}} = -\frac{\partial H}{\partial \mathbf{x}} \rightarrow \begin{cases} \dot{\boldsymbol{\lambda}}_r = -\mathbf{G}^\top \boldsymbol{\lambda}_v - \nabla G_r(\mathbf{r}) \\ \dot{\boldsymbol{\lambda}}_v = -\boldsymbol{\lambda}_r \\ \dot{\lambda}_m = u T_{max} / m^2 \boldsymbol{\lambda}_v \cdot \boldsymbol{\alpha} \end{cases} \tag{4.31}$$

with $\mathbf{G} = \partial \mathbf{g} / \partial \mathbf{r}$. In equations (4.4), the boundary conditions for the costates are all unknown except for λ_m. Since the final mass is free, its related costate must be zero

$$\lambda_m(t_f) = 0 \tag{4.32}$$

The conditions on the control variables u and $\boldsymbol{\alpha}$ are derived applying the Pontryagin Minimum Principle,

$$\boldsymbol{\alpha}^* = -\boldsymbol{\lambda}_v / \lambda_v \tag{4.33}$$

Applying the PMP to the Hamiltonian described above, it yields

$$\begin{cases} u^* = 0 & \text{if} \quad S_r > 0 \\ u^* \in [0,1] & \text{if} \quad S_r = 0 \\ u^* = 1 & \text{if} \quad S_r < 0 \end{cases} \tag{4.34}$$

being the radiation switching function S_r

$$S_r = -\lambda_v \frac{c}{m} - \lambda_m \tag{4.35}$$

Once the control variables have been determined, the augmented system can be expressed as

$$\dot{\mathbf{y}} = \mathbf{F}(\mathbf{y}) \rightarrow \begin{bmatrix} \dot{\mathbf{r}} \\ \dot{\mathbf{v}} \\ \dot{m} \\ \dot{\boldsymbol{\lambda}}_r \\ \dot{\boldsymbol{\lambda}}_v \\ \dot{\lambda}_m \end{bmatrix} = \begin{bmatrix} \mathbf{v} \\ \mathbf{g}(\mathbf{r}) - (\boldsymbol{\lambda}_v / \lambda_v) u T_{max} / m \\ -u T_{max} / c \\ -\mathbf{G}^\top \boldsymbol{\lambda}_v - \nabla G_r(\mathbf{r}) \\ -\boldsymbol{\lambda}_r \\ -\lambda_v u T_{max} / m^2 \end{bmatrix} \tag{4.36}$$

This system is completed by the boundary conditions described in equations (4.4) and (4.32). If an initial costate vector would be provided, one could integrate the equations over time and check if the terminal conditions are verified.

Theorem. The optimal throttle factor u^* is always equal to the unit in the radiation optimal transfer problem.

Proof. Given that $\lambda_v > 0$ because it represents a module, $\dot{\lambda}_m < 0$ by definition and taking into account equation (4.32), these two latter implies that $\lambda_m > 0$. Therefore, the switching function always reads negative values $S_r < 0$. Hence, according to equation (4.34), $u^* = 1$.

Therefore, according to [7]

Definition 7. Let $[\mathbf{x}(t), \boldsymbol{\lambda}(t)]^\top = \zeta([\mathbf{x}_i, \boldsymbol{\lambda}_i]^\top, t_i, t)$ be solution of equation (4.36) integrated from $[\mathbf{x}_i, \boldsymbol{\lambda}_i]^\top$, from the initial time t_i to a generic time t. The optimization problem is stated as follows:

$$\text{Find } \boldsymbol{\lambda}_i \text{ such that}$$

$$[\mathbf{x}(t_f), \boldsymbol{\lambda}(t_f)]^\top = \zeta([\mathbf{x}_i, \boldsymbol{\lambda}_i]^\top, t_i, t_f) \begin{cases} \mathbf{r}(t_f) - \mathbf{r}_f = 0 \\ \mathbf{v}(t_f) - \mathbf{v}_f = 0 \\ \lambda_m(t_f) = 0 \end{cases} \tag{4.37}$$

4.4 Shooting Methods

In the last Section, the radiation optimal trajectory problem has been fully explained and formulated. Once the procedure has been shown, the reader can notice that initialization values for the costates are necessary to integrate the equations over time prior to compare if the boundary conditions are satisfied. Usually, Newton's method is utilized to provide static values that optimize a certain Lagrangian function. However, in these cases, it is mandatory to add some sets of conditions (besides the original ones) to check if the solution provided by the solver is the desired one. If those conditions are not implemented, there is no way to guarantee that the selected point represents an absolute minimum/maximum of the functional. Generally, when shooting methods are introduced, they are mainly divided into two types: *single shooting* and *multiple shooting*. For the purpose of this work, the multiple shooting method has not been considered, so the current Section will focus entirely on the single shooting method for the sake of simplicity.

To keep it concise, the single shooting method attempts to solve a TPBVP by guessing the initial boundary conditions. A proper mathematical definition would read as follows [42]

Definition 8. *Methodology of the Single Shooting Method:* given the system of differential equations $\dot{\mathbf{x}}(t) = \mathbf{f}(\mathbf{x}(t), t)$ within the time interval $t_0 \leq t \leq t_f$. The unknown initial values $\mathbf{x}_0 = \mathbf{x}(t_0)$ will be determined in order to fulfill the terminal boundary condition $\boldsymbol{\Psi}(\mathbf{x}(t_f), t_f) = \mathbf{0}$.

When the TPBVP is obtained, then it is transformed into a set of equations of the form $\boldsymbol{\Gamma}(\boldsymbol{\lambda}_\mathbf{0}, t_f) = \mathbf{0}$, which is habitually referred to as shooting function. In this work, it is defined as

$$\boldsymbol{\Gamma}(\boldsymbol{\lambda}_\mathbf{0}, t_f) = \begin{bmatrix} \mathbf{r}(\boldsymbol{\lambda}_\mathbf{0}, t_f) - \mathbf{r}_f \\ \mathbf{v}(\boldsymbol{\lambda}_\mathbf{0}, t_f) - \mathbf{v}_f \\ \lambda_m(\boldsymbol{\lambda}_\mathbf{0}, t_f) \end{bmatrix} \tag{4.38}$$

Since the augmented system explained in last Section reads $\mathbf{y} = [\mathbf{x}, \boldsymbol{\lambda}]^\top \in \mathbb{R}^{14}$, the formulation of the TPBVP that needs to be solved is

$$\begin{aligned} \dot{\mathbf{y}} &= \mathbf{f}(\mathbf{y}), \quad t_0 \leq t_f \\ \mathbf{y}(t_0) &= [\mathbf{x}_0, \boldsymbol{\lambda}_0]^\top \\ \boldsymbol{\Psi}(\mathbf{y}(t_f)) &= 0 \end{aligned} \tag{4.39}$$

where the final time is known (by solving previously the minimum-time transfer problem for the same constraints). When an initialization value is given to the costates, the entire system of equations can be integrated over time through the following Initial Value Problem (IVP):

$$\begin{aligned} \dot{\mathbf{y}} &= \mathbf{f}(\mathbf{y}), \quad t_0 \leq t_f \\ \tilde{\mathbf{y}}(t_0) &= [\mathbf{x}_0, \tilde{\boldsymbol{\lambda}}_0]^\top \end{aligned} \tag{4.40}$$

This method gradually adjusts itself by the error committed in every iteration through Newton's method. In the solver provided by Politecnico di Milano used for the development of this thesis, the Runge-Kutta method has been used to integrate the trajectory of the spacecraft over time and, consequently, evaluate the shooting function.

4.5 Analytic Derivatives

The procedure explains through this Section focuses on the application of Newton's method to single shooting strategies in order to retrieve the analytic derivatives. This method employs the Jacobian of the shooting function $\mathbf{J}_\Gamma$ with respect to $\boldsymbol{\lambda}_0$ to compute in an iterative manner the initial guess of costates correcting inaccuracies at every step

$$\mathbf{J}_\Gamma = \frac{\partial \boldsymbol{\Gamma}}{\partial \boldsymbol{\lambda}_0} \tag{4.41}$$

$$\boldsymbol{\lambda}_0^{k+1} = \boldsymbol{\lambda}_0^k - \mathbf{J}_\Gamma^{-1} \boldsymbol{\Gamma}(\boldsymbol{\lambda}_0^k) \tag{4.42}$$

where the vector of costates is defined as states the equation (4.27).

Therefore, $\mathbf{J}_\Gamma \in \mathbb{R}^{7x7}$. As stated in [41], an advantage of this method lies in the fact that analytic derivatives are calculated instead of numerical ones. This matter highly affects the accuracy of this method. To handle the task of calculating the partial derivatives, the State Transition Matrix (STM) denoted as $\boldsymbol{\Xi}$. The STM is defined according to [41] as the mathematical tool that maps derivatives from one time to another on a given continuous trajectory.

$$\boldsymbol{\Xi}(t, t_0) = \frac{\partial \mathbf{y}(t)}{\partial \mathbf{y}(t_0)} \tag{4.43}$$

This yields to $\delta\mathbf{y}(t) = \Xi(t, t_0)\delta\mathbf{y}(t_0)$. The STM is obtained by the integration of

$$\frac{d\Xi(t, t_0)}{dt} = [\mathbf{J}_{\mathbf{f}(\mathbf{y})}]_t \Xi(t, t_0), \text{ being } \Xi(t_0, t_0) = \mathbf{I}_{14x14} \tag{4.44}$$

where $\mathbf{J}_{\mathbf{f}(\mathbf{y})} = \partial\mathbf{f}(\mathbf{y})/\partial\mathbf{y}$ represents the Jacobian of the equations of motion and $\mathbf{I}_{14x14}$ denotes the identity matrix in $\mathbb{R}^{14}$. Even though the introduction of the STM in the system ensures a higher accuracy to compute the derivatives, it also brings along some handicaps. The main one is the augmentation of the system from a $14x1$ state vector $\mathbf{y}$ to $210x1$ states. The first 14 are the original states of the augmented system and the rest of components belonging to the $14x14$ Ξ in array form. Consequently, the original problem is reconstructed to yield the final one as follows [7]

$$\dot{\mathbf{z}} = \mathbf{f}(\mathbf{z}) \rightarrow \begin{bmatrix} \dot{\mathbf{y}} \\ vec(\dot{\Xi}) \end{bmatrix} = \begin{bmatrix} \mathbf{f}(\mathbf{y}) \\ vec(\mathbf{\Gamma}_{\mathbf{f}(\mathbf{y})}\Xi) \end{bmatrix} \tag{4.45}$$

4.6 Structure of the Model

Last Section provided an overview about how to obtain the differential flux surfaces and how to approximate them. That module is going to be the core of all the computations made in the present analysis. Going one step further, it is needed to link the aforementioned module with the actual trajectory solver. The main goal of this Section is to present how this connection procedure has been carried out.

This linking process has been built mainly throughout three algorithms which are interconnected with each other. The first step consists in loading all the auxiliary variables such as energy vectors, differential fluxes fitted surfaces and RDC values (accordingly computed through the proton/electron energy vectors). Moreover, some initialization values must be considered for the total equivalent fluence (J_r), total equivalent flux (G_r) and total equivalent flux gradient ($\nabla\mathbf{G_r}$) at the first iteration, setting them to zero (scalar for the total equivalent fluence/flux and 3-component vector for the gradient).

The first algorithm (Algorithm 1) works as a history saver. Its inputs are: the trajectory history until the *i-th* iteration ($\mathbf{xx_h}$ covers until the $i-1$ iteration and xx_i covers the last one) and its related times ($\mathbf{t_h}$ and t_i, respectively), history arrays for the total equivalent fluences/fluxes ($\mathbf{J_h}$ and $\mathbf{G_{rh}}$), and history matrix of equivalent flux gradients ($\nabla\mathbf{G_{rh}}$). The auxiliary variables commented above are loaded as well in this module. Its outputs are: the updated history trajectory coordinates ($\mathbf{xx_{h2}}$), updated history times ($\mathbf{t_{h2}}$), updated history arrays for the total equivalent fluences/fluxes ($\mathbf{J_{h2}}$ and $\mathbf{G_{rh2}}$) and updated history matrix of equivalent flux gradients ($\nabla\mathbf{G_{rh2}}$).

Algorithm 1 History Saver Module.

1: update: $\mathbf{xx_{h2}} \leftarrow [\mathbf{xx_h} \;\; xx_i]$
2: update: $\mathbf{t_{h2}} \leftarrow [\mathbf{t_h} \;\; t_i]$
3: **procedure** EXECUTE ALGORITHM 2
4: update: $\mathbf{J_{h2}} \leftarrow [\mathbf{J_h} \;\; J_r + J_h(end)]$
5: update: $\mathbf{G_{rh2}} \leftarrow [\mathbf{G_{rh}} \;\; G_r]$
6: **procedure** EXECUTE ALGORITHM 3
7: update: $\nabla\mathbf{G_{rh2}} \leftarrow [\nabla\mathbf{G_{rh}} \;\; \nabla\mathbf{G_r}]$

The second block is the one responsible for calculating the shooting function at every step (total equivalent fluence at 1 MeV, J_r, and total equivalent flux at 1 MeV, G_r), which will be updated afterward in the Algorithm 1. This Shooting Function Module has been depicted in Algorithm 2. Its inputs are mainly a certain coordinates triad, a time span and the auxiliary variables. In the Algorithm 2, the total equivalent fluence at 1MeV has been computed integrating the respective proton/electron equivalent fluxes over the time span provided in the algorithm. In practice, this time span corresponds to the last two components of the updated history time array $\mathbf{t_{h2}}$. As seen in the Algorithm 2, its main function is calculating the total equivalent flux and fluence at 1 MeV. These values are passed to Algorithm 1 and its process continues.

Algorithm 2 Shooting Function Module.

1: compute linear/logarithmic altitude: $h_k, h_k^{log} = log(h_k)$
2: compute logarithmic energy vectors: $\mathbf{E_p^{log}} = log(\mathbf{E_p}), \mathbf{E_e^{log}} = log(\mathbf{E_e})$
3: build logarithmic altitude vector: $\mathbf{h^{log}}$
4: evaluate proton logarithmic differential flux at $\mathbf{h^{log}}$, $\mathbf{E_p^{log}}$: $log(\frac{d\boldsymbol{\phi}_p}{dE_p})$ Eq. (3.1)
5: evaluate electron logarithmic differential flux at $\mathbf{h^{log}}$, $\mathbf{E_e^{log}}$: $log(\frac{d\boldsymbol{\phi}_e}{dE_e})$ Eq. (3.2)
6: retrieve the linear differential protons/electrons flux vectors: $\frac{d\boldsymbol{\phi}_p}{dE_p}, \frac{d\boldsymbol{\phi}_e}{dE_e}$
7: integrate $\frac{d\boldsymbol{\phi}_p}{dE_p}$ over proton energy vector and multiply by α_{e-p} : G_r^p
8: integrate $\frac{d\boldsymbol{\phi}_e}{dE_e}$ over electron energy vector: G_r^e
9: compute total equivalent flux at 1MeV: $G_r = G_r^p + G_r^e$ Eq. (4.30)
10: compute total equivalent fluence at 1MeV: J_r

The last module consists in a block that calculates the gradient of the equivalent flux. It has been summarized in Algorithm 3. Its inputs are the trajectory

coordinates and the total equivalent fluxes at to consecutive steps. In particular, these consecutive steps corresponds to the last ones of the array. As an output, it provides the gradient of the aforementioned total equivalent flux.

Algorithm 3 Gradient Module.

1: calculate the total equivalent flux: $G_r(\mathbf{r})$
2: calculate the perturbed total equivalent flux: $G_r(\mathbf{r}+\epsilon)$ in x, y and z
3: calculate the gradient of $G_r(\mathbf{r}) : \nabla G_r(\mathbf{r}) = \frac{G_r(\mathbf{r}+\epsilon)-G_r(\mathbf{r})}{\epsilon}$

As it will be seen in Chapter 4, the gradient will be necessary to solve the dynamic set of equations which govern the problem. In order to get into the next iteration it is needed to update the next vectors:

$$\begin{aligned} \mathbf{xx_h} &= \mathbf{xx_{h2}} \\ \mathbf{t_h} &= \mathbf{t_{h2}} \\ \mathbf{J_h} &= \mathbf{J_{h2}} \\ \mathbf{G_{rh}} &= \mathbf{G_{rh2}} \\ \nabla\mathbf{G_{rh}} &= \nabla\mathbf{G_{rh2}} \end{aligned}$$

When the entire trajectory has been computed, then the vector $\mathbf{J_{h2}}$ contains the total equivalent fluence at 1 MeV at every single iteration. This variable accumulates over time. Therefore, at the last step, the total equivalent fluence at 1 MeV during the entire path can be retrieved.

4.7 Shortages of the Model

As anticipated in Section 3.2, most of the shortages of this model come as consequences of the assumptions and simplifications done. Obviously, the weakest point of this model is the fact that even though 3-D trajectories could be perfectly computed, it would not represent the problem under study due to the 2-D nature of the model. Consequently, trajectories with zero inclination should be considered. Another disadvantage of this model is that local information along the orbit is lost due to the averaged flux done afterwards. For example, this mainly affects if one wants to identify the South Atlantic Anomaly. Anyhow, that is not a major loss for the purposes of this research. There are also some sources of error related to this model. Maybe the clearest one comes motivated by the symmetry considered for the equatorial GEI plane. The latitude and longitude variation of few degrees between GEI and MAG (quantified in Figure 2.5) also compose a source of errors. Another important shortage of this model, even though justified to prioritize speed, is the fact that it has not got a temporal dependency. In other words, it is fixed

in the time in which the computational design is done, i.e. the period between the 1st of January 2018 and 92 days after. Another source which could induce errors is the spacial grid made, even though is pretty tight for the purposes of this work (~40 km). For more detailed known issues in AE9/AP9 models, the reader is referred to [47].

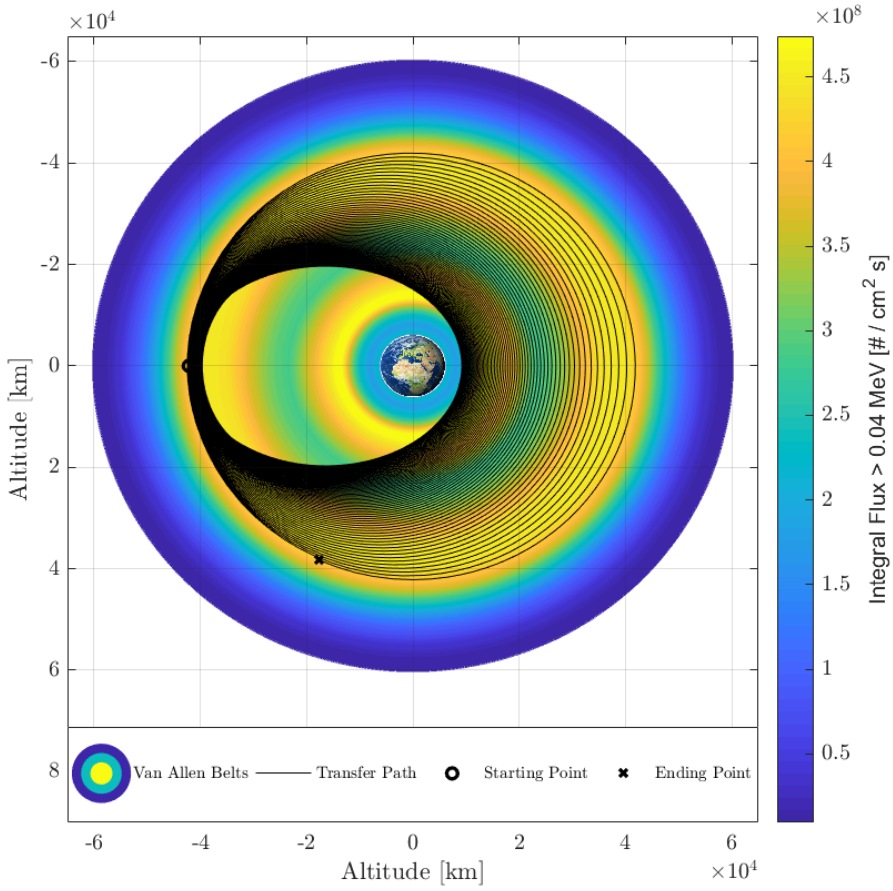

FIGURE 4.1: Transfer baseline example.

4.8 Validations

The main goal of this Section is to ensure that the radiation model built throughout this Chapter represents faithfully the behavior of Van Allen Belts environment. In order to do that, a general transfer must be taken as a baseline example. The one taken in this validation process has been depicted in Figure 4.1, where a time optimal trajectory computed by LT2O is represented.

There is a wide variety of possibilities to validate the developed model that has been developed. As it respects to this research, the checking procedure

has been mainly carried out through two representative variables; the differential fluence and the total equivalent fluence at 1 MeV. The results have been double checked with SPENVIS (total equivalent fluence at 1 MeV) and AE9/AP9/SPM (differencial fluence).

In Figure 4.2, a comparison between differential fluences for both electrons and protons considering the transfer path described above has been depicted. The similarity between trends validates the model under evaluation. This result was expected regarding the fact that the developed model has been extracted from AE9/AP9/SPM software. Nevertheless, it was worth to compute this outputs considering the assumptions and simplifications made for the model's development. As the reader can notice, the hypotheses taken beforehand are verified accordingly by the results.

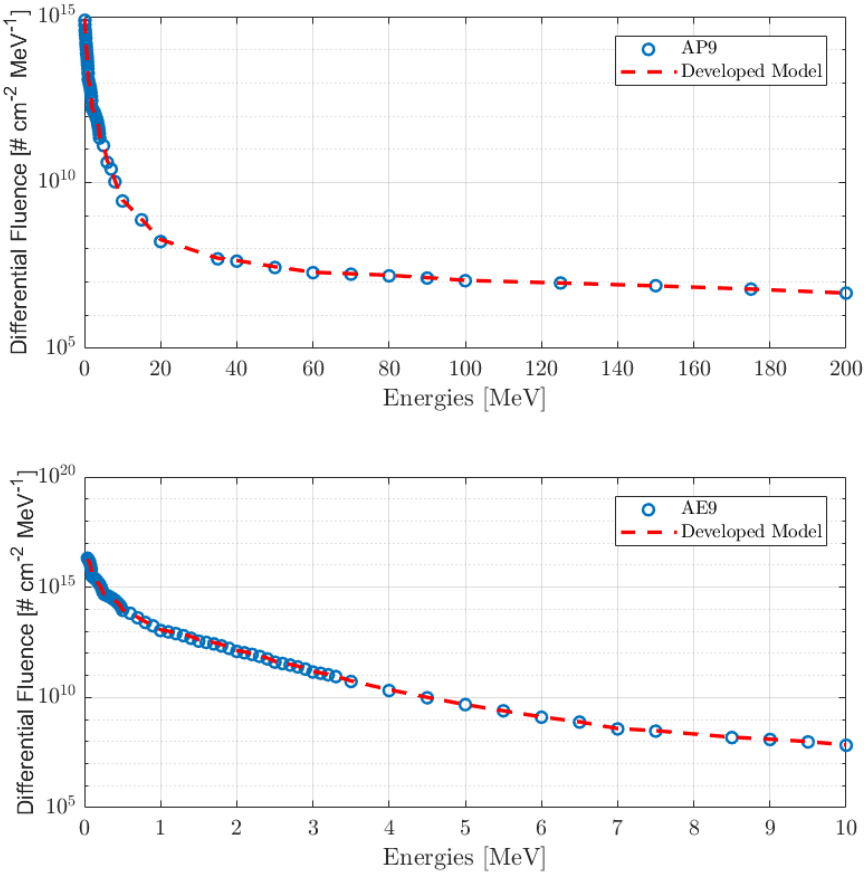

FIGURE 4.2: Differential fluence comparison for protons (top) and electrons (bottom).

Analogously, the current validation would not be completed without comparing the main variable in this research; the total equivalent fluence at 1 MeV. This variable is, as commented several times during this thesis, the total equivalent fluence at 1 MeV. It has been depicted in Figure 4.3 against

coverglass thicknesses of the solar cell. One can realize that the values obtained for low coverglass thicknesses are pretty accurate while they diverge a bit when coverglass thickness increases. This is due to the fact that the solar cell degradation model in Figure 3.2 is not pretty accurate. Nevertheless, all the computations regarding this work consider 1 mils coverglass thickness. Therefore, the errors committed as a result of this fact are minimized.

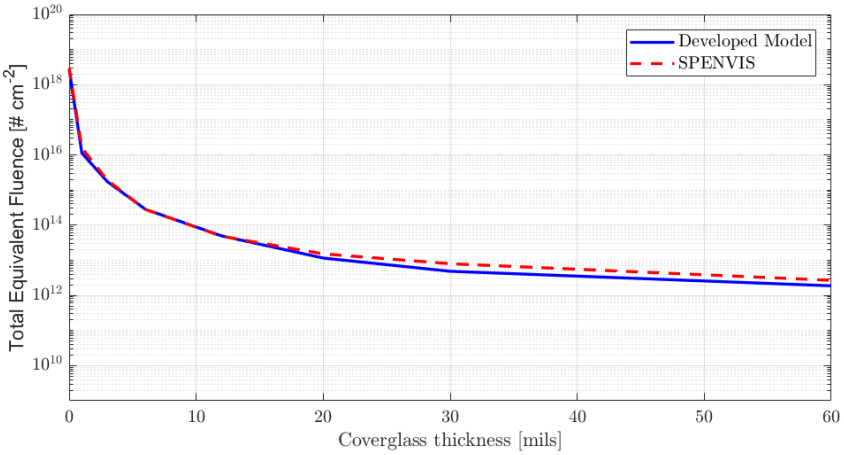

FIGURE 4.3: Total Equivalent Fluence at 1 MeV comparison.

4.9 Preliminary Numerical Analysis

In the current Section, the theory that has been explained beforehand is applied in a real scenario. The radiation optimal problem has been attempt to be solved for a LEO to GEO transfer for the parameters given in Table 4.1.

TABLE 4.1: Parameters for the Preliminary Analysis.

Parameter	Value
Mass [kg]	1000
Thrust [N]	20
Specific Impulse [s]	3000
Time [days]	90

It is important that the reader notices about the preliminary character of this analysis. Hence, this study holds a symbolic meaning over the ones reported in this thesis. In any case, the solver did not converge for this analysis after a long trial-error procedure varying thrust and/or TOF. Consequently, the thesis is expected to serve as a reference for following researches on this topic, since no results could have been generated.

Chapter 5

Conclusions

"Anyone who has never made a mistake has never tried anything new."

- Albert Einstein, *1879 - 1955*

The main contribution of this thesis is to create a fast and reliable radiation model which is meant to be incorporated into an optimization framework in order to determine minimum equivalent fluence transfers. To that end, this thesis provides the groundwork for future researches about this topic, and moreover, a first approach to an architecture capable of minimizing a certain performance index different from TOF and propellant expenditure. During this work, the next objectives have been reached:

- To understand the advantages of electric propulsion compared to other kinds of technologies.
- To comprehend the behavior of Van Allen Belts and its associated mechanisms.
- To model the Van Allen Belts in an efficient manner.
- To implement the aforementioned model into a solver.
- To learn how optimal control works for orbital transfers.

As long as the model developed to represent the Van Allen Belts has resulted to be very robust and its outputs pretty accurate, its implementation into the solver has not worked the way it was expected at the beginning. Some major difficulties have been found when the low-thrust condition has been imposed. As a result, only a preliminary numerical solution has been shown forcing a high-thrust transfer. In any of the cases, it is expected to serve to the scientific community as a preliminary manual taking into account the drawbacks that it brings along.

There are many ways of improving the developed procedure. Some of this features would be:

- Selection of a finer altitudes grid to get more accurate results in the developed model.
- Addition of other sources of radiation such as galactic cosmic rays or solar particle events.
- Implementation of new solar cells to check the impact on the overall mission.
- Last and most importantly, the implementation of a module to be incorporated in LT2O that solves the radiation optimal problem derived.

Bibliography

[1] J.G. del Amo, "Electric Propulsion in Space Missions", in *EPIC Workshop*, 2017.

[2] G.A. Landis, S.R. Oleson, and C.R. Mercer, "Solar Electric Propulsion for Future NASA Missions", in *42nd IEEE Photovoltaic Specialists Conference (PVSC)*, 14-19 Jun. 2015; New Orleans, LA; United States, 2015.

[3] M. Kim, "Continuous low-thrust trajectory optimization: techniques and applications", *PhD Thesis*, Virginia Tech, 2005.

[4] J.A. Sims, P.A. Finlayson, E.A. Rinderle, M.A. Vavrina, and T.D. Kowalkowski, "Implementation of a Low-Thrust Trajectory Optimization Algorithm for Preliminary Design", *American Institute of Aeronautics and Astronautics*, 2006.

[5] L.D. Berkovitz and N.G. Medhin, "Nonlinear Optimal Control Theory", *Chapman and Hall/CRC*, 2012.

[6] N.R. Morón, "Indirect Optimization of Electric Propulsion Orbit Raising to GEO with Homotopy", *MSc Thesis*, Politecnico di Milano, 2017.

[7] C. Zhang, F. Topputo, F. Bernelli-Zazzera, and Y.S. Zhao, "Low-thrust minimum-fuel optimization in the circular restricted three-body problem", *Journal of Guidance, Control and Dynamics*, 38(8): 1501-1510, 2015.

[8] J.W. Howard and D.M. Hardage, "Spacecraft Environments Interactions: Space Radiation and Its Effects on Electronic Systems", *NASA Journal*, Alabama, 1999.

[9] L. Ferella, "Indirect Optimization of Long-Duration, Multi-Spiral Low-Thrust Transfers with Homotopy", *MSc Thesis*, Politecnico di Milano, 2016.

[10] J. Gonzalo, F. Topputo, and R. Armellin, "Indirect optimization of end-of-life disposal for galileo constellation using low thrust propulsion", *26^{th} International Symposium on Space Flight Dynamic*, 3-9 June 2017.

[11] G. Genta and P.F. Maffione, "Optimal low-thrust trajectories for nuclear and solar electric propulsion", *Acta Astronautica*, Volume 118, pages 251-261, 2016.

[12] L.D. Edmonds, C.E Barnes, and L.Z. Scheick, "An Introduction to Space Radiation Effects on Microelectronics", *JPL Publication*, Pasadena, California, 2000.

[13] M.A. Xapsos, J.L. Barth, E.A. Burke, and G.B. Gee, "Space Environment Effects: Model for Emission of Solar Protons (ESP) - Cumulative and Worst-Case Event Fluences", *NASA Journal*, Alabama, 1999.

[14] A. Dutta, N.J. Kasdin, and E. Choueiri, "Minimizing Proton Displacement Damage Dose During Electric Orbit Raising of Satellites", *Journal of Guidance, Control and Dynamics*, Volume 39, No 4, April 2016.

[15] R. Jehn, "Radiation optimum solar-electric-propulsion transfer from GTO to GEO", *24th International Symposium On Space Flight Dynamics*, 2014.

[16] A. Dutta, P. Libraro, N.J. Kasdin, and E. Choueiri, "Minimum-Fuel Electric Orbit-Raising of Telecommunication Satellites Subject to Time and Radiation Damage Constraints", *American Control Conference (ACC)*, June 4-6, Portland, Oregon, 2014.

[17] H. Garrett, "Guide to Modeling Earth's Trapped Radiation Environment", *AIAA-Reston*, Virginia, 1999.

[18] A. Dutta, S. Vijayan, and T. Olson, "Deployment of High Power Class All-Electric Satellites in the Geosynchronous Equatorial Orbit", *AIAA Space Forum*, 13 - 16 September, Long Beach, California, 2016.

[19] C.R. Koppel, "Low Thrust Orbit Transfer Optimiser for a Spacecraft Simulator", *6th International Conference on Astrodynamics Tools and Techniques (ICATT)*, Darmstadt, 15-17 March, 2016.

[20] M. Willis and S. D'Amico, "Analytical approach to spacecraft formation-flying with low-thrust relative spiral trajectories", *Acta Astronautica*, 2017.

[21] S. Schäff and A. Wiegand, "Advanced Electric Orbit-Raising Optimization for Operational Purpose", *25th International Symposium on Space Flight Dynamics*, Munich, Germany, 2015.

[22] L. Mazzini, "Finite thrust orbital transfers", *Acta Astronautica*, Volume 100, 107–128, 2014.

[23] S. Ceccherini, L. Ferella, and F. Topputo, "Assessment of hybrid propulsion for geostationary transfer orbits: a mission design approach", *67th International Astronautical Congress*, 16(C1.4.8), Guadalajara, Mexico, 2016.

[24] G. Mingotti, F. Topputo, and F. Bernelli-Zazzera, "Transfers to distant periodic orbits around the Moon via their invariant manifolds", *Acta Astronautica*, Volume 79, Pages 20-32, 2012.

[25] G. Mingotti, F. Topputo, and F. Bernelli-Zazzera, "Efficient invariant-manifold, low-thrust planar trajectories to the Moon", *Communications in Nonlinear Science and Numerical Simulation*, Volume 17, Issue 2, Pages 817-831, 2012.

[26] Y. Lian, Y. Gao, and G. Tang, "On equatorial inclination of parking orbits in transfers to lunar halo orbits", *Communications in Nonlinear Science and Numerical Simulation*, Volume 28, Issues 1–3, Pages 210-222, 2015.

[27] H. Zeng and J. Zhang, "Modeling low-thrust transfers between periodic orbits about five libration points: Manifolds and hierarchical design", *Acta Astronautica*, Volume 145, Pages 408-423, 2018.

[28] C.A. Kluever, "Optimal low-thrust, Earth-Moon trajectories", *PhD Thesis*, Iowa State University, 1993.

[29] J. Olympio, "Optimisation and optimal control methods for planet sequence design of low-thrust Interplanetary transfer problems with gravity-assists", *PhD Thesis*, École Nationale Supérieure des Mines de Paris, 2009.

[30] X.L. Hellín, "Study of Earth-to-Mars Transfers with Low-Thrust Propulsion", *MSc Thesis*, Universitat Politécnica de Catalunya, 2011.

[31] L.L. Sackett, H.L. Malchow, and T.N. Edelbaum, "Solar Electric Geocentric Transfer With Attitude Constraints: Analysis", *NASA Journal*, 1975.

[32] S. Bourdarie and M. Xapsos, "The Space Radiation Environment", *IEEE Trans. in Nucl. Sc. (TNS)*, 2008.

[33] M. Sajid, N.G. Chechenin, F.S. Torres, M.N. Hanif, U.A. Gulzari, S. Arslan, E.U. Khan, "Analysis of Total Ionizing Dose effects for highly scaled CMOS devices in Low Earth Orbit", *Nuclear Instruments and Methods in Physics Research Section B: Beam Interactions with Materials and Atoms*, Volume 428, Pages 30-37, 2018.

[34] M. Schulz, "Geomagnetically Trapped Radiation", *Space Science Reviews*, 1975.

[35] D.K. Srinivasan, N. Adams, R. Wallis, "In-flight performance of the Van Allen Probes RF telecommunications system", *Acta Astronautica*, Volume 116, Pages 211-221, 2005.

[36] M.K Hudson, B.T. Kress, H.R. Mueller, J.A. Zastrow, and J.B. Blake, "Relationship of the Van Allen radiation belts to solar wind drivers", *Journal of Atmospheric and Solar-Terrestrial Physics*, volume 70, 708-729, 2008.

[37] S. Ceccherini, "Methodology for System-Trajectory Optimization of Hybrid Transfers to the Geostationary Orbit", *Politecnico di Milano*, Chapter 5, 2018.

[38] M.A. Hapgood, "Space physics coordinate transformations: A user guide", *Planetary and Space Science*,Volume 40, Issue 5, 711-717, 1992.

[39] S.R. Messenger, G.P. Summers, E.A. Burke, R.J. Walters, and M.A. Xapsos, "Modeling solar cell degradation in space: A comparison of the NRL displacement damage dose and the JPL equivalent fluence approaches", *Progress in Photovoltaics: Research and Applications*, Volume 9, Issue 2, 2001.

[40] Y. Ren, "Low-Thrust Trajectory Optimization", *Department of Applied Mathematics I*, Universitat Politecnica de Catalunya.

[41] R.P. Russell, "Primer vector theory applied to global low-thrust trade studies", *Journal of Guidance, Control, and Dynamics*, 30(2):460-472, 2007.

[42] B. A. Conway, "Spacecraft Trajectory Optimization", *Cambridge University Press*, 2010.

[43] U.S Naval Observatory, "Almanac for Computers 1990", *Nautical Almanac Office, U.S. Naval Observatory*, Washington, D.C., 1989.

[44] C. Roth, "IRENE: AE9/AP9/SPM Radiation Environment Model, User Guide", *Air Force Research Laboratory*, V1.50.001, 2017.

[45] A. E. Bryson, "Applied optimal control: optimization, estimation and control", *CRC Press*, 1975.

[46] J. M. Longuski, J. J. Guzmán, and J. E. Prussing, "Optimal control with aerospace applications", volume 32, *Springer Science and Business Media*, 2013.

[47] R. Johnston, "IRENE: AE9/AP9/SPM Radiation Environment Model, Known Issues and Limitations", *Air Force Research Laboratory*, V1.50.001, 2017.

[48] S. R. Messenger, F. Wong, B. Hoang, C. D. Cress, R. J. Walters, C. A. Kluever, and G. Jones, "Low-Thrust Geostationary Transfer Orbit (LT2GEO) Radiation Environment and Associated Solar Array Degradation Modeling and Ground Testing", volume 32, *IEEE Transactions on Nuclear Science*, Vol. 61, 2014.

[49] T. P. O'Brien, "AE9/AP9 Guidance for Third-Party Developers", *Space Science Applications Laboratory*, 2014.

[50] L. S. Pontryagin, "Mathematical theory of optimal processes", *Routledge*, 2018.